AEDC-TR-67-222

A THEORETICAL AND EXPERIMENTAL INVESTIGATION OF A SPHERICAL GAS JOURNAL BEARING

A. E. Hodapp, Jr.
ARO, Inc.

October 1967

VON KÁRMÁN GAS DYNAMICS FACILITY
ARNOLD ENGINEERING DEVELOPMENT CENTER
AIR FORCE SYSTEMS COMMAND
ARNOLD AIR FORCE STATION, TENNESSEE

NOTICES

When U. S. Government drawings specifications, or other data are used for any purpose other than a definitely related Government procurement operation, the Government thereby incurs no responsibility nor any obligation whatsoever, and the fact that the Government may have formulated, furnished, or in any way supplied the said drawings, specifications, or other data, is not to be regarded by implication or otherwise, or in any manner licensing the holder or any other person or corporation, or conveying any rights or permission to manufacture, use, or sell any patented invention that may in any way be related thereto.

Qualified users may obtain copies of this report from the Defense Documentation Center.

References to named commercial products in this report are not to be considered in any sense as an endorsement of the product by the United States Air Force or the Government.

A THEORETICAL AND EXPERIMENTAL INVESTIGATION OF A SPHERICAL GAS JOURNAL BEARING

A. E. Hodapp, Jr.

ARO, Inc.

AF - AEDC
Arnold AFS Tenn

FOREWORD

The research presented herein is sponsored by the Arnold Engineering Development Center (AEDC), Air Force Systems Command (AFSC), Arnold Air Force Station, Tennessee, under Program Element 6540223F, Project 06RB.

The work presented herein was obtained by ARO, Inc. (a subsidiary of Sverdrup & Parcel and Associates, Inc.), contract operator of AEDC, AFSC, under Contract AF 40(600)-1200. The work was conducted under ARO Project No. VT8002, and the manuscript was submitted for publication on September 26, 1967.

This report was submitted to the University of Tennessee Space Institute as partial fulfillment of the requirements for a Master of Science degree.

The author wishes to express his appreciation to Dr. J. Lukasiewicz, Mr. C. J. Schueler, and Mr. L. K. Ward, of ARO, Inc., and the Arnold Engineering Development Center, U.S. Air Force, for their permission to use the experimental work as material for the thesis. The author is particularly indebted to Mr. Schueler for suggesting the thesis topic and for his many encouragements. Thanks are also due Mr. C. T. Bell for his valuable assistance with computer programming; and to Dr. W. T. Snyder for his assistance in the preparation and review of the thesis.

This technical report has been reviewed and is approved.

Donald H. Meyer
Major, USAF
AF Representative, VKF
Directorate of Test

Leonard T. Glaser
Colonel, USAF
Director of Test

ABSTRACT

An externally pressurized spherical gas journal bearing, which has multiple spherically surfaced pads, was designed and fabricated for use as a three degree-of-freedom pivot which will support large loads (100 lbs). This inherently compensated pool type bearing design proved to be pneumatically unstable. The problem then was to determine a restrictor configuration for this bearing which would insure pneumatic stability and a large load carrying capacity. Restrictor configurations investigated were inherent compensating both with and without a pool and orifice compensating without a pool.

The Reynolds equation and the equations for the distributed film velocities are developed in the report for spherical coordinates. Using these equations, theoretical estimates of bearing pad static characteristics (load carrying capacity, stiffness, etc.) were obtained for the above listed restrictor configurations. The problem of pneumatic instability was investigated using information available in the literature. The operating conditions of the bearing are such that the theoretical predictions are subject to question. A model bearing, which duplicates the lubricating film of a journal bearing pad, was, therefore, constructed in order to obtain experimental data to verify the theoretical predictions.

For this particular bearing configuration operating at large supply pressures (800 psig), it was found that an inherent compensating restrictor without a pool will ensure pneumatic stability and maximum load carrying capacity. This result is in agreement with theoretical predictions of dynamic behavior and is in disagreement with theoretical predictions of load carrying capacity.

TABLE OF CONTENTS

LIST OF FIGURES

NOMENCLATURE

A	Area, $in.^2$
B	Bearing parameter (Equation 20)
C	Normalized constant radial clearance (film thickness), c/h_r
C_d	Discharge coefficient
c_p	Specific heat at constant pressure, $in.^2/sec.^2-{}^oR$
c	Constant radial clearance (film thickness), in.
d	Orifice diameter for inherent compensation; secondary pool diameter for orifice compensation, in.
d_o	Orifice diameter, in.
G	Eccentricity function, $\sin\theta(1 - \varepsilon\cos\theta)^3$
H	Normalized radial clearance (film thickness), h/h_r
h	Radial clearance (film thickness), in.
I	Variable (Equation 33)
K	Constant
K_A, K_D	Constants, $lb.^2/in.^4$
K_n	Knudsen number, λ/h
k	Thermal conductivity, $lb.-sec./{}^oR$
L_A, L_D	Constants
L_S	Radial surface line length of arc, in.
M	Mach number
m	Mass flow, $lb.\ sec.^2/in.-sec.$
P	Normalized pressure, p/p_2

p	Pressure, lb./in.^{2}
R	Bearing pad radii, in.
Re^*	Modified film Reynolds number, $\rho\bar{u}h^2/L_s\mu$
$\mathfrak{R}$	Gas constant, in.^{2}/sec.^{2}-^oR
r	Spherical coordinate radius ($r_B + z$), in.
r_B	Radius of model bearing ball, in.
S	Normalized film stiffness, $sh_r/\pi(r_B \sin\theta)^2 p_2$
s	Film stiffness lb./in.
T	Temperature, ^oR
T_ω	Normalized time, ωt
t	Time, sec.
U	Normalized velocity in the θ-direction, u_h/v_r
u	Velocity in the θ-direction, in./sec.
V	Normalized velocity in the φ-direction, v_h/v_r
v	Velocity in the φ-direction, in./sec.
W	Normalized bearing load carrying capacity, $w/\pi r_B^2(\sin\theta)^2 p_2$
w	Bearing load carrying capacity, lb.
w'	Velocity in the r-direction, in./sec.
z	Distance measured in the r-direction from the surface of the ball ($0 \leq z \leq h$), in.
Γ	Normalized density, ρ/ρ_2
γ	Ratio of specific heats
δ	Pool depth, in.
δ^*	Secondary pool depth, in.

ε Eccentricity ratio, 1-h/c

ξ Variable (Equation 35)

Θ Normalized bearing coordinate, θ/θ_2

θ Spherical coordinate, rad.

Λ Compressibility number, $6\mu_2 r v_r / h_r^2 p_2$

λ Mean free molecular path, in.

μ Absolute viscostiy, lb.-sec./in.^{2}

ρ Density, lb. sec.^{2}/in.^{4}

σ Squeeze number, $12\mu_2 r^2 \omega / h_r^2 p_2$

τ Tangent ratio, $\tan(\theta/2)/\tan(\theta_2/2)$

Ω Normalized viscosity, μ/μ_2

φ Spherical coordinate, rad.

ω Reference circular frequency, rad./sec.

$(\bar{\ })$ Average value

$(\dot{\ })$ First derivative with respect to time

Subscripts

c Critical flow conditions; i.e., conditions at which the restrictor flow is sonic

F Film conditions

h Condition at z = h

M Maximum conditions

R Restrictor conditions

r Reference conditions

S Supply conditions

1	Conditions at the entrance to the bearing film
2	Conditions at the bearing film exit (ambient)

CHAPTER I

INTRODUCTION

I. BACKGROUND INFORMATION

In recent times a demand has arisen for the development of multi-degree-of-freedom methods for evaluating the rigid body dynamics of model aerodynamic configurations in wind tunnels. In answer to this demand, a three degree-of-freedom captive model dynamic stability balance was developed. The pivot of this balance, a spherical gas journal bearing, is the subject of this thesis. Gas bearings are desirable for this application due to their extremely low friction (1)[1]. As shown in Figure 1, this gas bearing consists mainly of an outer movable bearing housing to which models are attached, and an inner fixed bearing core through which gas is supplied to the bearing surfaces. The inner core has machined on it four spherically surfaced pads arranged in a manner which allows the journal bearing to both resist loads in any radial direction and center itself. One pad faces forward and the remaining three pads are located 120 degrees apart each being located 109.5 degrees

---

[1]Numbers in parentheses refer to similarly numbered references in the bibliography.

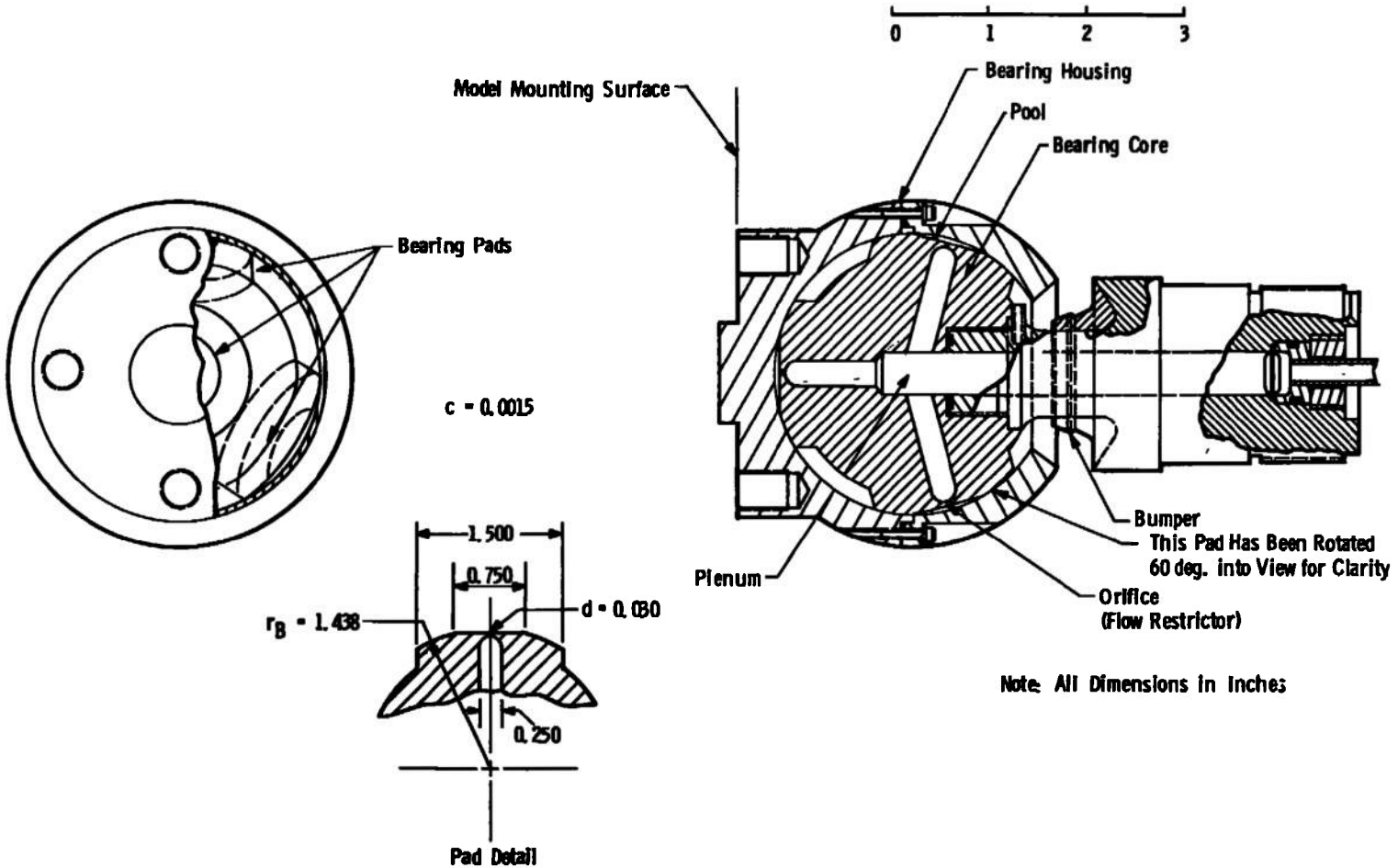

Figure 1. Journal bearing.

from the forward facing pad. The bearing allows unlimited angular freedom about its axis of symmetry and ±10 degrees of angular freedom about any transverse axis through its center. All of these capabilities are necessary for its application.

Gas flows under pressure from the plenum through each orifice (flow restrictor) then radially outward along the surface of each pad through the clearance between the bearing core outer diameter and the bearing housing inner diameter. The resistance to gas flow through the thin clearance over each pad produces a pressure gradient which results in a force in the gas film which acts to keep the bearing core and housing separated. As the clearance (film thickness) decreases the resistance to flow increases thus decreasing the mass flow and consequently the pressure drop across the flow restrictor. Since the pressure drop across the restrictor decreases with decreasing mass flow, the force generated in the gas film increases with decreasing clearance. This effect, known as compensation, will be discussed later in Chapter III. The type of compensation is denoted by the type of flow restrictor.

II. STATEMENT OF THE PROBLEM

Unfortunately this gas bearing proved to be pneumatically unstable (see page 79). The task of determining

the modifications necessary to make it operable was assigned to the author. It was decided that the only practical modification that could be made to this bearing, without completely machining the bearing surfaces, would be to change the restrictor configuration. A restrictor configuration was sought which would provide both high load capacity and stiffness while insuring pneumatic stability. A secondary consideration in the choice of a restrictor configuration would be to obtain a low value of the mass flow. The bearing restrictor was to be designed for the use of nitrogen since a high pressure dry nitrogen supply system exists in the facility where this bearing will be used. The methods used in determining the restrictor configuration, and the information obtained in this effort form the subject matter of this thesis.

The geometry of this bearing makes it very difficult to analyze using existing theoretical analyses like those developed by Pan (2). A method was sought which could be more easily applied. In the axial direction (along the axis of symmetry) the journal bearing can be approximated as one consisting of two identical spherically surfaced pads horizontally opposed. Although this simplified theoretical model cannot be used to determine the maximum journal bearing load capacity in any radial direction, it does allow the use of single pad load capacity versus radial clearance

characteristic curves in evaluating the relative load capacity and stiffness produced by different journal bearing restrictor configurations.

In order to develop the pad characteristics for use with this model, and to gain a more thorough understanding of gas lubrication theory, a basic theoretical study was performed. Using methods similar to those which Gross (3) used to develop the gas lubrication equations in cartesian coordinates, equations for the distributed film velocities and the isothermal Reynolds equation were developed in spherical coordinates (Appendix A). From these a set of equations was developed which describe the static characteristics of spherically surfaced bearing pads (Chapter III). Existing theoretical analyses were used to evaluate the problem of pneumatic instability.

As a result of the small pad sizes, and the elevated operating pressures necessary to gain load carrying capacity, the validity of the viscous isothermal theoretical predictions was questioned. An experimental investigation was therefore conducted using a model representative of one bearing pad to obtain data for comparison with theoretical predictions.

CHAPTER II

APPARATUS

I. MODEL BEARING

The purpose for fabricating the model bearing shown in Figure 2 was to obtain a simple means by which an experimental evaluation could be made of the performance of restrictor configurations proposed for the journal bearing pads. The model bearing was designed such that its lubricating film will be a duplicate of the film geometry over a journal bearing pad. The model bearing pad is concave while the journal bearing pads are convex and the pools are shaped differently; however; these differences should have a negligible effect on the relative performance. Both the pad diameter and pool diameter (Figure 2) of this spherical pad bearing are identical to those of the journal bearing (Figure 1, page 2). The spherical surface of this pad was obtained by lapping a 2.875 inch diameter hardened chrome alloy precision steel sphere into it. This method of construction caused the constant radial clearance of the model to be smaller than that of the journal bearing. The constant radial clearance of the model bearing was determined to be approximately 0.0005 inches. This is approximately one third the constant radial clearance of the journal bearing

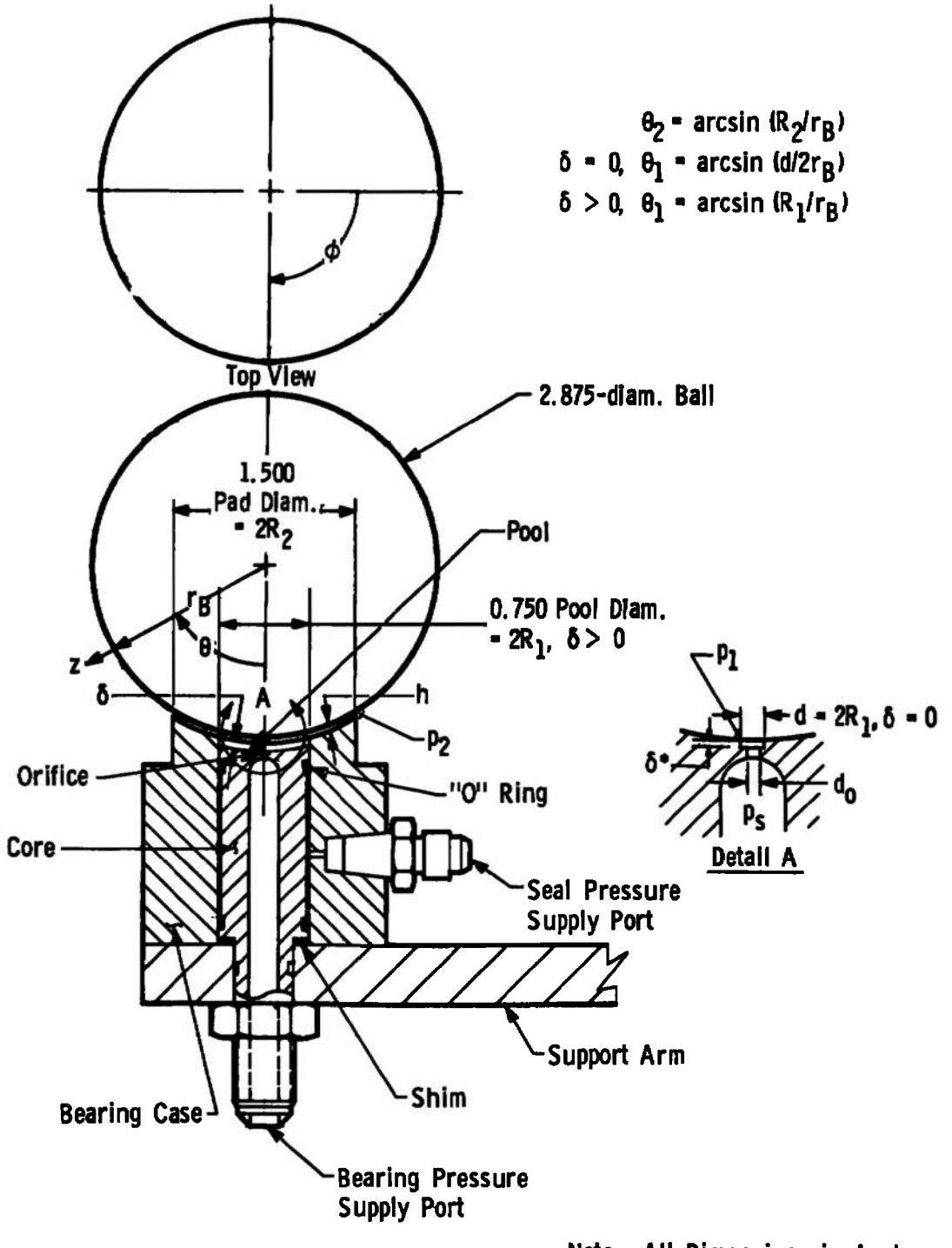

Figure 2. Model bearing.

pads; therefore, at clearances where the model bearing is operating near zero eccentricity, the journal bearing will be operating at large eccentricities.

The model bearing pool volume can be varied from zero to an excess of the clearance volume by a movable core which is positioned through the use of shims. An undesirable consequence of making this core movable is the volume which results from the difference in the core outer diameter and the bearing case inner diameter. This increases the pool volume which increases the chance of pneumatic instability. In an effort to minimize this volume, the bearing was designed with the following features:

1. The diametrical clearance between the two parts was held below 0.0003 inches.
2. An "O"-ring seal was placed as close to the bearing surface as possible.
3. Seal pressure was applied to force the "O"-ring into the upper portion of its grove.

The model bearing was designed to operate at seal pressures and gas supply pressures up to 1000 psia. Gas is supplied to the bearing clearance through an orifice located in the hollow core. Orifice sizes and configurations were changed by modifying the core section.

II. CALIBRATION APPARATUS

The experimental apparatus, shown schematically in Figure 3, is designed so that loads can be applied to the model bearing along its axis of symmetry and the resulting axial deflections determined. This apparatus consists of the model bearing, a load bracket, calibration weights, and a dial indicator with its support.

The load bracket consists of two flat circular disks connected by three metal columns. The top disk has a circular opening in it which is contoured to fit the ball and allows the ball to protrude through it. The bottom disk has a hook located at its center from which the calibration weights are suspended. This allows the load vector of the calibration weights to lie approximately along the bearing axis of symmetry.

The dial indicator is aligned to read deflections along the bearing axis of symmetry. It reads off that portion of the ball which protrudes through the upper load bracket disk. The dial indicator support is attached to the bearing case to insure accuracy in the deflection measurements.

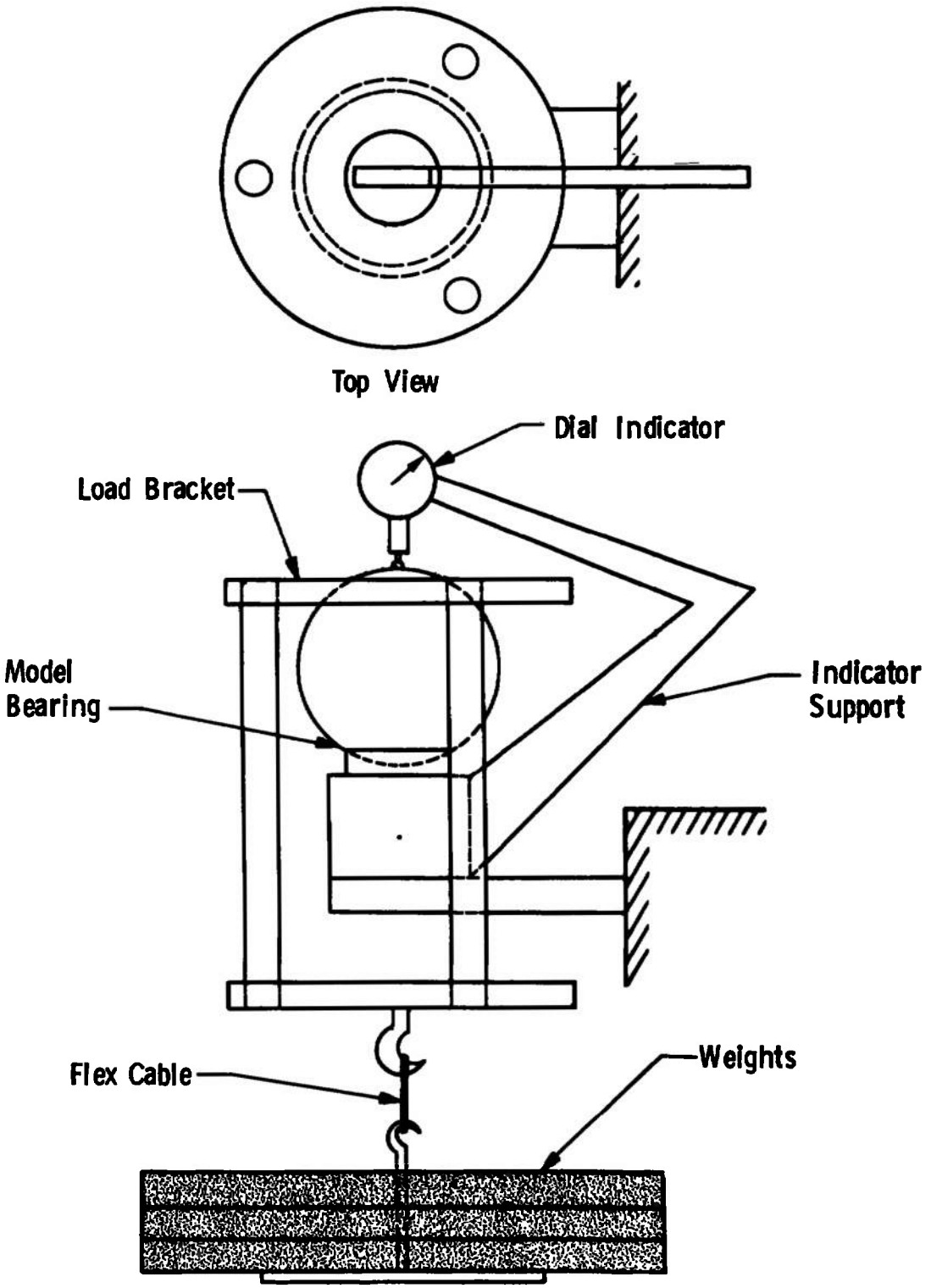

Figure 3. Calibration apparatus.

CHAPTER III

THEORETICAL ANALYSIS AND DISCUSSION

This chapter will be used to develop the relations which are fundamental in the design of a hydrostatic spherical bearing pad of the type shown in Figure 2, page 7. It will be assumed that the bearing surfaces remain concentric and that there is no relative motion between them. These conditions eliminate the pressure gradient in the φ direction; therefore, the equations given in Appendix A for the velocity distribution in the viscous film (Equations A-10 and A-11) reduce to

$$u = \frac{1}{2\mu r} \frac{dp}{d\theta} z\left[z - h\right], \tag{1}$$

$$v = 0,$$

and the normalized viscous isothermal Reynolds equation (Equation A-14) becomes

$$\frac{d}{d\theta}\left[(\sin\theta)\, H^3 P\right]\frac{dP}{d\theta} = 0. \tag{2}$$

These equations together with information from existing references will be used to develop the relations for the

mass flow, inlet pressure, pressure distribution, load capacity and stiffness. These relations will be developed primarily for the case of constant radial clearance; however, more general forms of some will be investigated.

An analysis of air hammer or pneumatic instability will not be presented. The information contained in References (4) through (9) will be used to identify the responsible parameters and their undesirable trends. The geometries of the configurations considered in these references do not match the geometry of the present configuration; however, they are sufficiently close, so that the predicted trends should be valid.

I. FLOW RESTRICTORS

Certainly the external flow restrictor is one of the more important portions of a hydrostatic gas bearing. It produces the gas film stiffness, which enables the bearing to compensate for changes in load. Restrictors used in these bearings may be grouped in three basic categories:

1. Laminar restrictors,
2. Fixed orifice restrictors (orifice compensation), and
3. Variable or inherent orifice restrictors (inherent compensation).

A fourth possible type, which will not be considered, is a variable servomechanism device. Figure 4 gives the geometries of the flow restrictors listed above.

Laminar restrictors, which include both capillary and porous restrictors, are less desirable than the remaining types as they are more susceptible to pneumatic instability and also because they provide less stiffness while operating at the same supply pressure (10). For these reasons laminar restrictors will not be considered in the following analysis.

Only orifice type restrictors will be considered in the following study. For orifice compensation the fixed orifice area ($A_R = \pi d_o^2/4$) is the restrictor. In the case of inherent compensation the circumference of the orifice together with the variable clearance height form the restricting area ($A_R = \pi dh$). Using Figure 5, page 15, the following expressions can be written for the possible restricting areas formed by a circular orifice for bearing configurations with and without a pool.

Case 1, Pool ($\delta > 0$):

1a. $A_R = \pi d_o^2/4$,

1b. $A_R = \pi d\left[h + \delta\right]$,

1c. $A_R = \pi d_o\left[h + \delta + \delta^*\right]$, and

1d. $A_R = 2\pi R_1 h$.

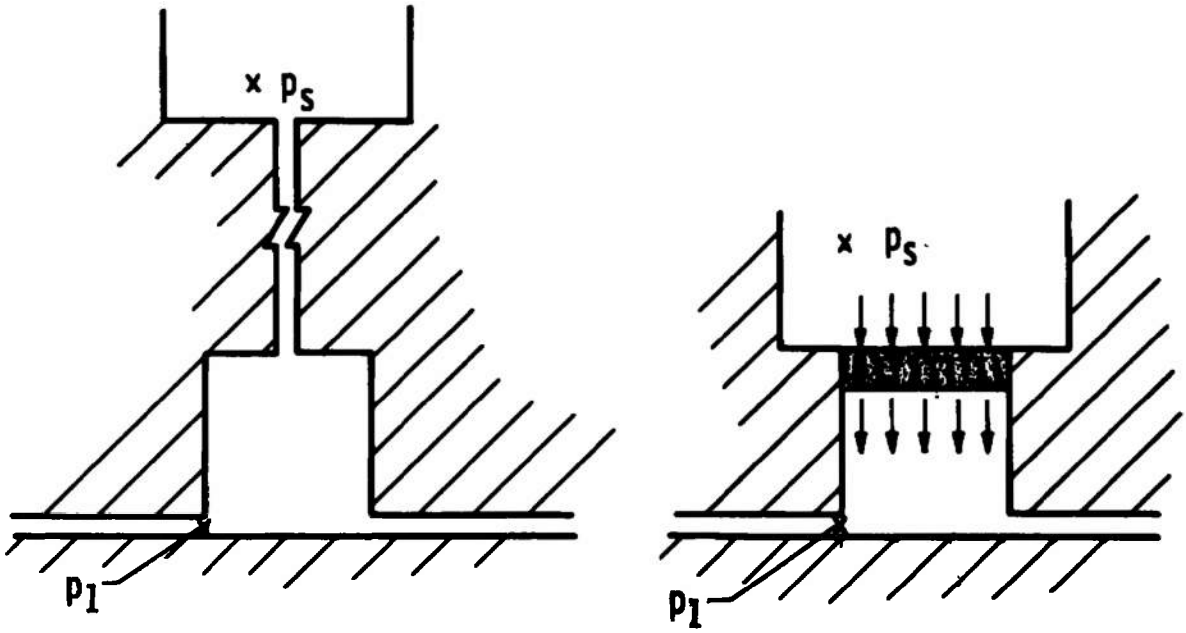

a. Laminar restrictors.

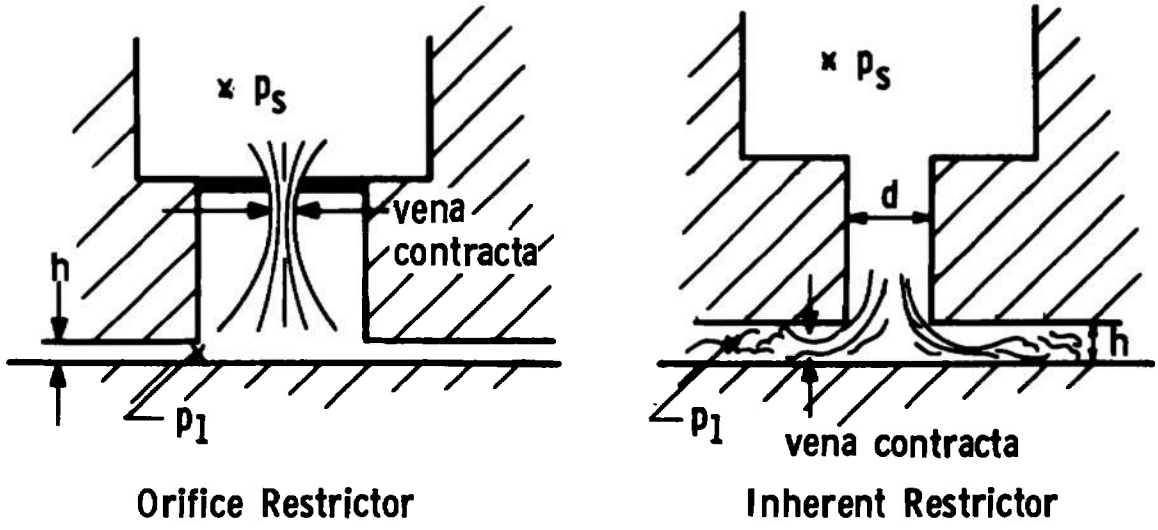

b. Fixed and variable orifice restrictors.

Figure 4. Bearing flow restrictor configuration.

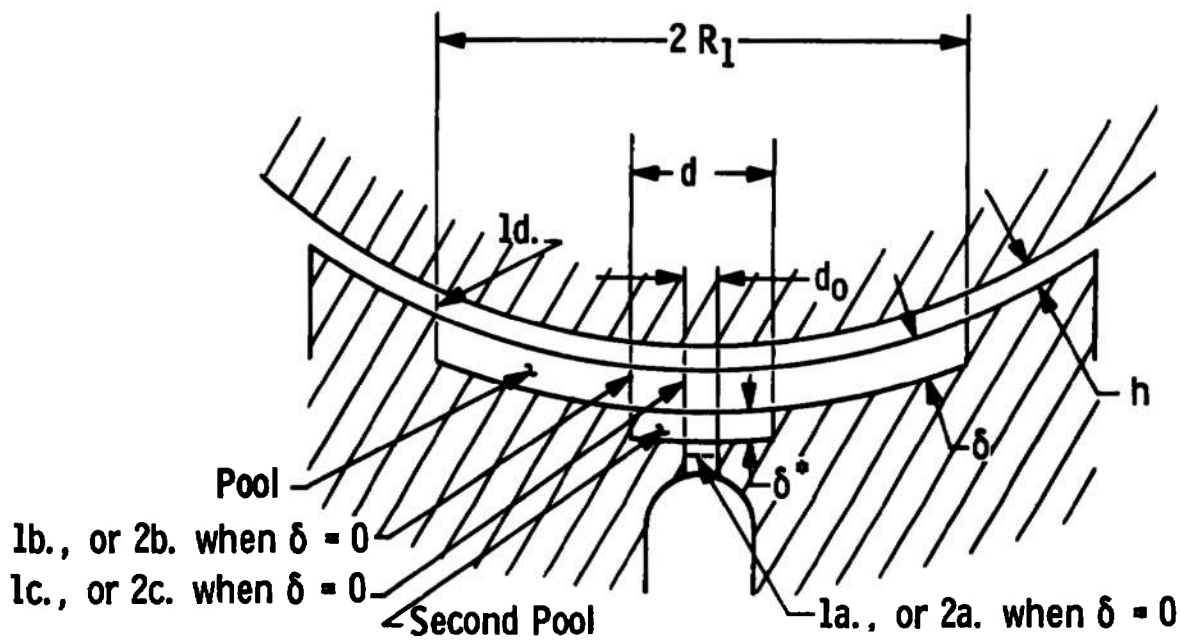

Figure 5. Possible orifice type restrictors.

Case 2, No Pool ($\delta = 0$):

2a. $A_R = \pi d_o^2/4$,

2b. $A_R = \pi dh$, and

2c. $A_R = \pi d_o\left[h + \delta^*\right]$.

Only cases 1a, 1b, 2a, and 2b will be considered. Cases 1c and 2c must be taken into consideration when attempting to design an orifice restrictor. Case 1d is undesirable for our purposes due to the possibility of high mass flows. For most pool bearings $R_1 \gg d$.

The conditions which ensure orifice compensation are as follows:

With $\delta = 0$,

$d > d_o^2/4h_{min}$ (A_R for 2a < A_R for 2b),

$\delta^* > d_o/4 - h_{min}$ (A_R for 2a < A_R for 2c).

With $\delta > 0$,

$d > d_o^2/4\left[h_{min} + \delta\right]$ (A_R for 1a < A_R for 1b),

$\delta^* > d_o/4 - \left[\delta + h_{min}\right]$ (A_R for 1a < A_R for 1c).

where h_{min} is the minimum expected radial clearance over an orifice.

For many pool bearings

$$d_o/4 - \left[\delta - h_{min} \right] > 0;$$

therefore, a second pool is required to obtain orifice compensation (Figure 5, page 15). This feature is often undesirable due to the resulting increase in pool volume.

II. MASS FLOW

In order to describe the mass flow through a hydrostatic bearing it is necessary to develop separate relations for the flow through the restrictor and the flow through the bearing clearance. For the assumed case of no relative surface motion the mass flow through these separate portions is equal when the gas flow is steady.

Restrictor flow. The gas flow through the restrictor is assumed to be one-dimensional and isentropic. For these conditions Reference (11) gives the following relations for a perfect gas which can be combined to form a theoretical expression for the mass flow.

$$m_R = \rho_R \bar{u}_R A_R \ , \tag{3}$$

$$p_R = \rho_R R T_R \ , \tag{4}$$

$$a_R = \sqrt{\gamma R T_R} \ , \tag{5}$$

$$\bar{u}_R = M_R a_R \ , \tag{6}$$

$$\frac{T_R}{T_S} = \left[1 + \frac{(\gamma - 1)}{2} M_R^2\right]^{-1} \ , \tag{7}$$

$$\frac{p_R}{p_S} = \left[1 + \frac{(\gamma - 1)}{2} M_R^2\right]^{\frac{-\gamma}{(\gamma-1)}} \ . \tag{8}$$

Rearranging Equations 4, 5, and 6, and then substituting into Equation 3,

$$m_R = A_R p_R M_R \sqrt{\frac{\gamma}{RT_R}} \ .$$

Solve Equation 8 for M_R; then substitute the result and Equation 7 into the above expression. After some algebraic manipulation

$$m_R = A_R p_S \left\{ \frac{2\gamma}{(\gamma - 1)RT_S} \left[\left(\frac{p_R}{p_S}\right)^{\frac{2}{\gamma}} - \left(\frac{p_R}{p_S}\right)^{\frac{(\gamma+1)}{\gamma}} \right] \right\}^{\frac{1}{2}} \ . \tag{9}$$

Equation 9 is corrected for deviations from the theoretical assumptions by multiplying it by the experimentally determined discharge coefficient which is defined as

$$C_d = \frac{\text{Actual mass flow}}{\text{Theoretical mass flow (Equation 9)}} .$$

The mass flow through the restrictor for unchoked flow is, therefore, given as

$$m_R = A_R p_S C_d \left\{ \frac{2\gamma}{(\gamma - 1)RT_S} \left[\left(\frac{p_R}{p_S} \right)^{\frac{2}{\gamma}} - \left(\frac{p_R}{p_S} \right)^{\frac{\gamma+1}{\gamma}} \right] \right\}^{\frac{1}{2}} . \tag{10}$$

The critical pressure ratio, or pressure ratio that initiates sonic flow through the restrictor, is obtained by letting $M_R = 1$ in Equation 8,

$$P_c = \left[\frac{p_R}{p_S} \right]_c = \left[\frac{2}{(\gamma + 1)} \right]^{\frac{\gamma}{\gamma-1}} . \tag{11}$$

For constant A_R, p_S, and T_S, the mass flow remains constant when $p_R/p_S \leq P_c$; therefore, for choked flow, the mass flow through the restrictor is

$$m_R = A_R p_S C_d \left\{ \frac{2\gamma}{(\gamma - 1)RT_S} \left[P_c^{\frac{2}{\gamma}} - P_c^{\frac{\gamma-1}{\gamma}} \right] \right\}^{\frac{1}{2}} . \tag{12}$$

Bearing flow. For the bearing configuration under consideration the mass flow through the clearance is in the

θ-direction. A relationship describing this condition may be derived by using the expression

$$m_F = \rho_F \bar{u}_F A_F \ , \tag{13}$$

where $\bar{u}_F$ is the average film velocity at a particular cross section of the clearance whose area is A_F. Using Equation 1 the average velocity for the viscous laminar film is obtained as follows:

$$\bar{u}_F = \frac{2}{3} u_M \quad \text{(parabolic velocity profile)} \ ,$$

$$u = u_M \quad \text{at} \quad z = \frac{h}{2} \ ;$$

therefore,

$$\bar{u}_F = \frac{-h^2}{12\mu r} \frac{dp}{d\theta} \ . \tag{14}$$

Since the radius of curvature (r_B) is large compared to the film thickness (h) the cross sectional area of the film, as a function of θ, may be written as

$$A_F = 2\pi r h \sin \theta \ .$$

Substituting this expression and Equation 14 into Equation 13 yields

$$m_F = - \frac{\pi}{6} \left[\frac{h^3 \sin \theta}{\mu} \rho \frac{dp}{d\theta} \right] . \qquad (15)$$

For steady flow conditions this equation may be differentiated with respect to θ to yield the θ-component of the Reynolds equation

$$\frac{d}{d\theta} \left[\frac{h^3 \sin \theta}{\mu} \rho \frac{dp}{d\theta} \right] = 0 .$$

This approach to obtaining the Reynolds equation has been used by many authors. Pan (2) derived the steady flow Reynolds equation in spherical coordinates using this method.

Substituting the equation of state (Equation A-8) into Equation 15 results in

$$m_F = \frac{-\pi h^3 \sin \theta}{6 R \mu T} p \frac{dp}{d\theta} . \qquad (16)$$

For a constant radial clearance (h = const.) and steady viscous isothermal flow

$$(\sin \theta) p \frac{dp}{d\theta} = K_A . \qquad (17)$$

Integrating

$$\frac{p^2}{2} = K_A \ln \tan \left(\frac{\theta}{2} \right) + K_D .$$

Using the above equation and the boundary conditions

$$p = p_1 \quad \text{at } \theta = \theta_1 ,$$

$$p = p_2 \quad \text{at } \theta = \theta_2 ,$$

(see Figure 2, page 7) K_A is determined to be

$$K_A = \frac{-\left(p_1^2 - p_2^2\right)}{2 \ln\left[\dfrac{\tan\left(\dfrac{\theta_2}{2}\right)}{\tan\left(\dfrac{\theta_1}{2}\right)}\right]} .$$

Combining this relation with Equations 16 and 17

$$m_F = \frac{-\pi h^3\left[p_1^2 - p_2^2\right]}{12\mu RT \ln \tau_1} , \tag{18}$$

where

$$\tau_1 = \frac{\tan\left(\dfrac{\theta_1}{2}\right)}{\tan\left(\dfrac{\theta_2}{2}\right)} .$$

III. FILM INLET PRESSURE

In developing an expression for the inlet pressure to the film, the following assumptions will be made:

1. h = constant,

2. $p_1 \simeq p_R$, and

3. $T \simeq T_S$.

It should be noted that some of the kinetic energy imparted to the flow as it exits the restrictor is recovered and is not completely lost as assumed (assumption 2); therefore, $p_1 > p_R$ and $T_R < T < T_S$. The second assumption given above yields sufficiently accurate results for many problems; however, the pressure recovery should be taken into consideration when designing a bearing to attain a particular stiffness level and mass flow at a given supply pressure. Vohr has demonstrated this in References (10) and (12). The third assumption given above, which is widely used in the literature, is in error at most 17 per cent when nitrogen is used.

Assuming that the mass flow is constant, Equations 10 and 18 can be equated and rearranged to obtain:

$$\left(\frac{p_1}{p_S}\right)^2 - 1 = B\,\frac{p_S}{p_2}\left[\left(\frac{p_1}{p_S}\right)^{\frac{2}{\gamma}} - \left(\frac{p_1}{p_S}\right)^{\frac{\gamma+1}{\gamma}}\right]^{\frac{1}{2}}. \qquad (19)$$

The bearing parameter (B) is defined as:

$$B = \frac{-12\mu C_d \ln(\tau_1)}{\pi p_2}\left[\frac{A_R}{h^3}\right]\sqrt{\frac{2\gamma RT_S}{(\gamma - 1)}} \quad . \tag{20}$$

The normalized inlet pressure for unchoked restrictor flow is obtained from Equation 19 after some algebraic manipulation as:

$$P_1 = \left\{1 + BP_S^{\frac{\gamma-1}{2\gamma}} P_1^{\frac{1}{\gamma}}\left[P_S^{\frac{\gamma-1}{\gamma}} - P_1^{\frac{\gamma-1}{\gamma}}\right]^{\frac{1}{2}}\right\}^{\frac{1}{2}} \quad . \tag{21}$$

Using the same approach, the expression for P_1 at the choked restrictor condition can be obtained and is given as:

$$P_1 = \left\{1 + BP_S P_c^{\frac{1}{\gamma}}\left[1 - P_c^{\frac{\gamma-1}{\gamma}}\right]^{\frac{1}{2}}\right\}^{\frac{1}{2}} \quad , \tag{22}$$

where for a given type gas P_c is a constant defined by Equation 11. Equations 21 and 22 were given previously by Tang and Gross (13).

The bearing parameter at which the flow becomes choked (B_c) is obtained by substituting the identity

$$P_1 = P_c P_S$$

into Equation 22 and rearranging terms to get

$$B_c = \frac{P_c^2 P_S^2 - 1}{P_S P_c^{\frac{1}{\gamma}} \sqrt{1 - P_c^{\frac{\gamma-1}{\gamma}}}}$$

for choked flow $B \leq B_c$.

The functional dependence of the normalized inlet pressure is given as[1]

$$P_1 = P_1(B, P_S, \gamma).$$

Figure 6 gives P_1 as a function of B and γ at constant P_S for both choked and unchoked flows. Effects of changing P_S are not shown in this fugure; however, as would be expected P_1 increases with increasing P_S.

IV. PRESSURE PROFILES

In this section pressure profiles for viscous isothermal flow will be developed. The bearing configuration under consideration may be operated at pressures which violate these flow conditions; therefore, a portion of this section will be used to describe the effects that fluid inertia (viscous-inertial flow) and compressibility (inviscid supersonic flow) have on the assumed viscous pressure profile.

---

[1]Letters contained in parentheses following a parameter indicate the functional dependence of that parameter.

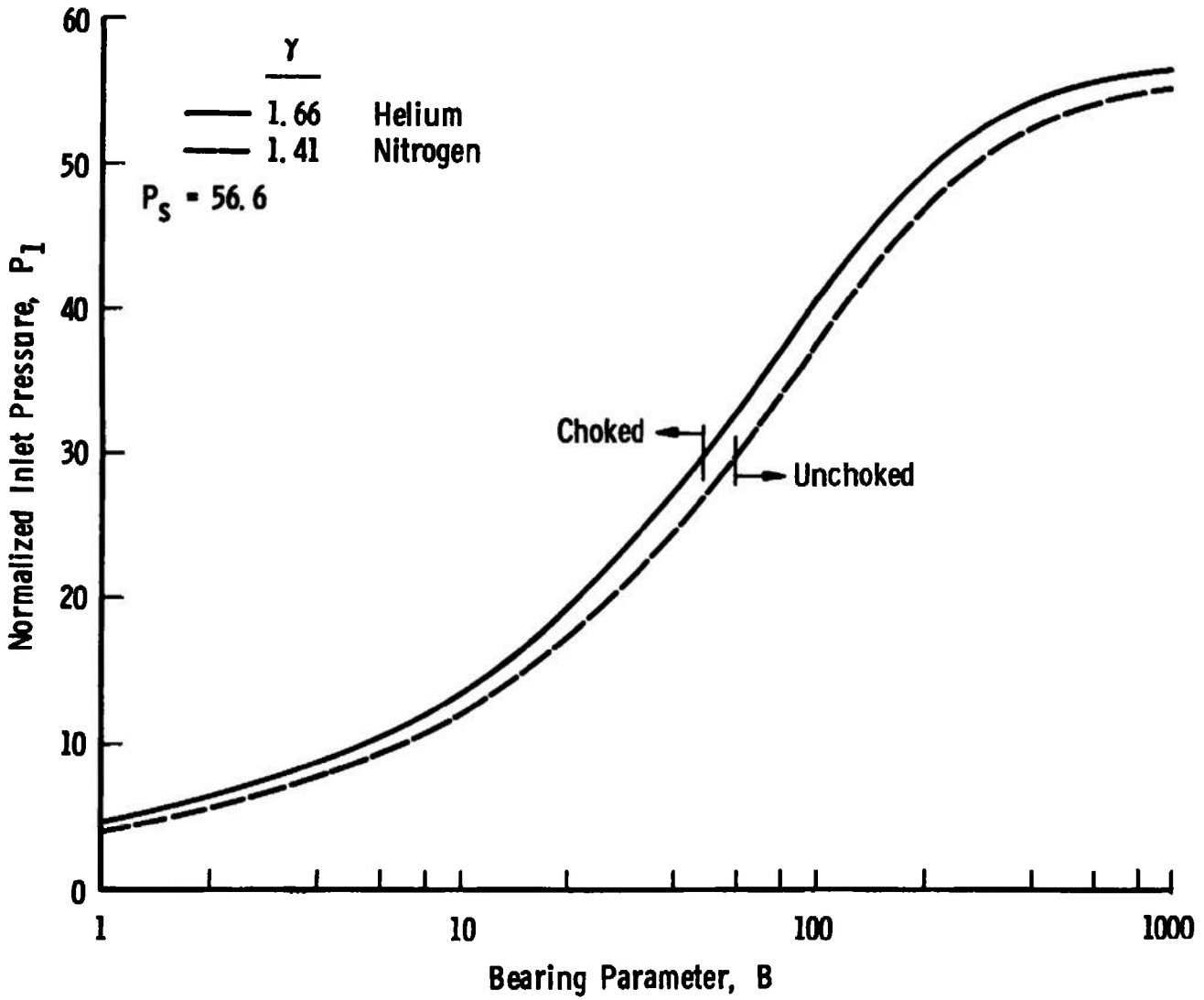

Figure 6. Theoretical bearing film inlet pressure.

Constant radial clearance. For the bearing configuration under consideration operating under conditions of constant radial clearance (h = c = const.) and viscous isothermal flow, Equation 2 reduced to

$$\frac{d}{d\theta}\left[(\sin\theta)\ P\ \frac{dP}{d\theta}\right] = 0\ ; \tag{23}$$

therefore,

$$(\sin\theta)\ P\ \frac{dP}{d\theta} = L_A\ .$$

The normalized pressure is obtained by integrating this equation

$$\frac{P^2}{2} = L_A\ \ln\tan\left(\frac{\theta}{2}\right) + L_D\ . \tag{24}$$

Using this equation and the boundary conditions

$$P = P_1 \quad \text{at } \theta = \theta_1\ ,$$

$$P = 1 \quad \text{at } \theta = \theta_2\ ,$$

(see Figure 2, page 7) the constants L_A and L_D are determined to be

$$L_A = \frac{\left[P_1^2 - 1\right]}{2\ \ln\tau_1}\ ,$$

$$L_D = \frac{1}{2}\left[1 - \frac{\left[P_1^2 - 1\right]}{\ln \tau_1} \ln\left(\frac{\tau}{\tau_1}\right)\right]^{\frac{1}{2}} .$$

The following expression for the normalized film pressure is obtained after substituting the above constants in Equation 24 and rearranging terms

$$P = P_1\left[1 + \frac{\left[P_1^2 - 1\right]}{P_1^2 \ln \tau_1} \ln\left(\frac{\tau}{\tau_1}\right)\right]^{\frac{1}{2}} , \qquad (25)$$

where

$$\tau = \frac{\tan\left(\frac{\theta}{2}\right)}{\tan\left(\frac{\theta_2}{2}\right)} .$$

When the radial clearance is constant,

$$P = P(\theta, \tau, B, \gamma, r_B, P_S).$$

Figure 7 gives the theoretical pad pressure distributions which demonstrate the trends of the pressure when P_S and R_2 are held constant. The magnitude of the pressure is increased by decreasing θ. For a bearing with fixed radius of curvature (r_B) the area under pressure curve is increased by increasing B, τ_1, γ, and P_S. Holding the inner and outer

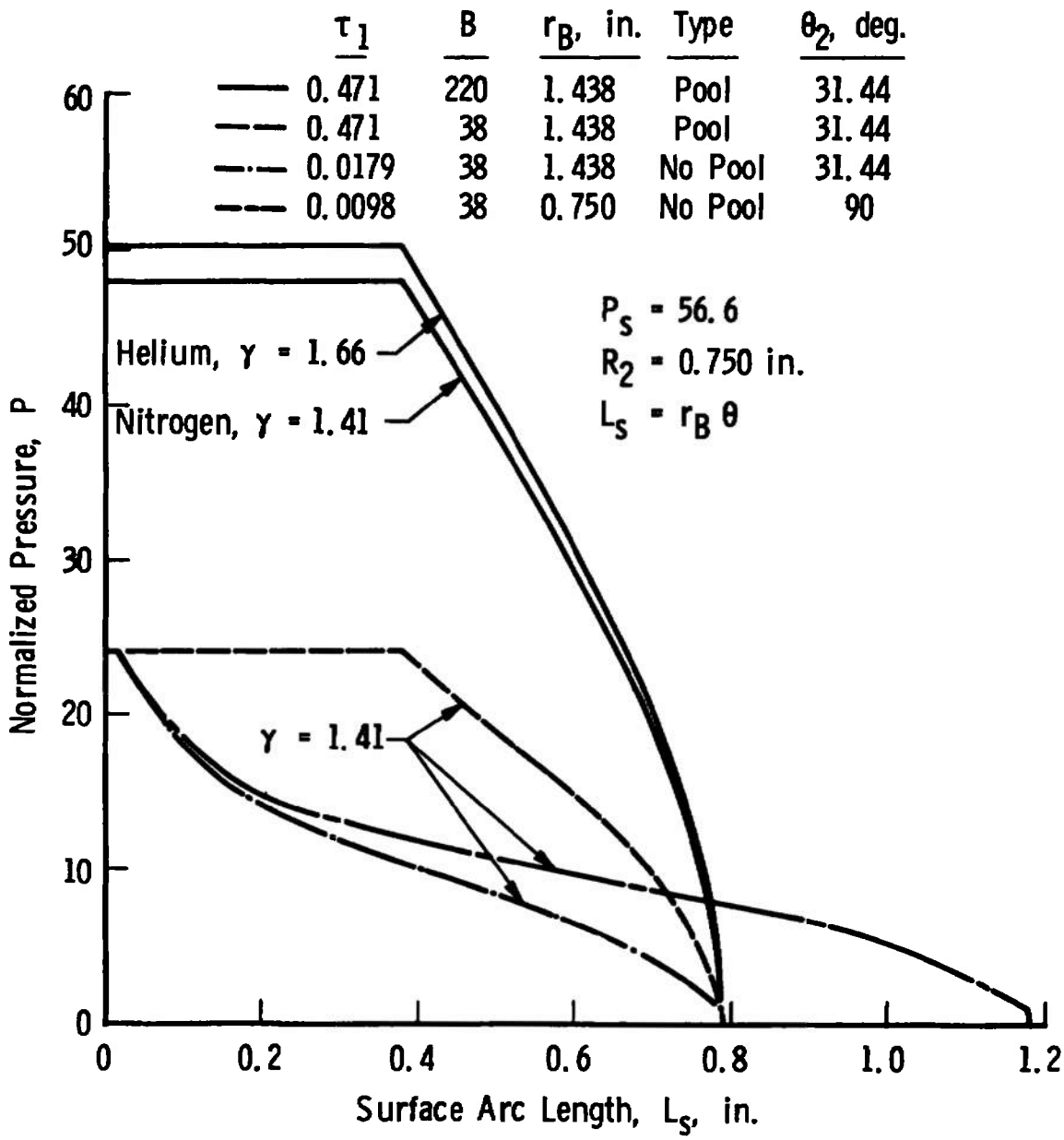

Figure 7. Theoretical pad pressure profiles.

boundary radii (R_1 and R_2) fixed and decreasing the radius of curvature results in increased surface area. Even though τ_1 is decreased using this procedure, the area under the pressure curve is increased, thereby increasing the load carrying capacity of the bearing.

Variable radial clearance. A more general pressure profile is obtained by letting the radial clearance vary in the θ-direction. This situation is shown graphically in Figure 8 where the radial clearance is given as

$$h = c\left[1 - \varepsilon \cos \theta\right].$$

The eccentricity ratio (ε) is defined at $\theta = 0$ as

$$\varepsilon = 1 - \frac{h}{c} .$$

The radial clearance relation given above is normalized by dividing through by h_r to get

$$H = C\left[1 - \varepsilon \cos \theta\right] .$$

Recalling Equation 2 we can write

$$\left(\sin \theta\right) H^3 P \frac{dP}{d\theta} = K .$$

Substituting Equation 26 into this relation and integrating using the bearing inlet conditions as a reference:

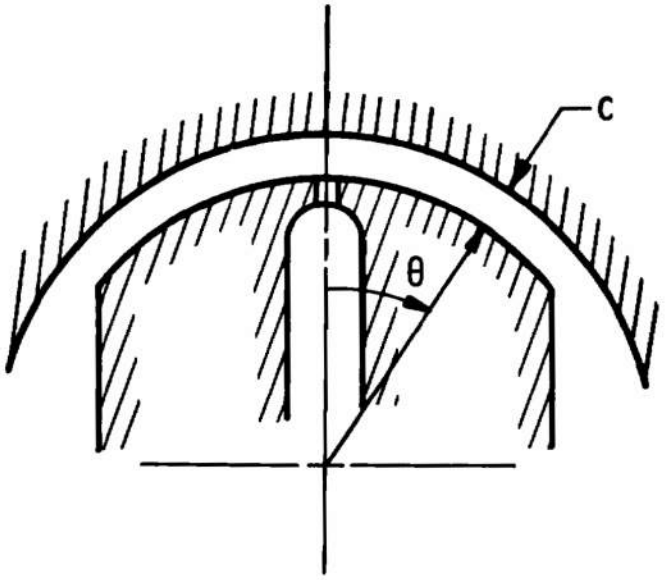

a. Constant radial clearance, h = c.

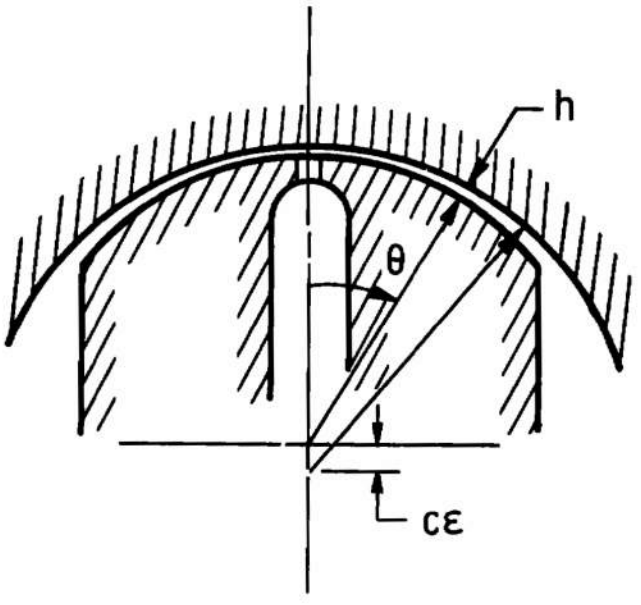

b. Variable radial clearance, h = c(1 - ε cos θ).

Figure 8. Bearing film geometry.

$$P^2 = P_1^2 + \frac{2K}{C^3} \int_{\theta_1}^{\theta} \frac{d\theta}{\sin \theta \left[1 - \varepsilon \cos \theta\right]^3} \quad . \qquad (27)$$

For nonzero ε numerical integration techniques were used to evaluate the above integral.

Using the above equation and the normalized boundary conditions given on page 27, the constant K is determined to be:

$$K = \frac{C^3\left[1 - P_1^2\right]}{2} \left[\int_{\theta_1}^{\theta_2} \frac{d\theta}{\sin \theta \left[1 - \varepsilon \cos \theta\right]^3} \right]^{-1} \quad .$$

Substituting this constant into Equation 27 yields the following expression for the normalized film pressure

$$P = P_1 \left[1 + \frac{\left[1 - P_1^2\right]}{P_1^2 \int_{\theta_1}^{\theta_2} G(\theta)\, d\theta} \int_{\theta_1}^{\theta} G(\theta)\, d\theta \right]^{\frac{1}{2}} , \qquad (28)$$

where

$$G(\theta) = \frac{1}{\sin \theta \left[1 - \varepsilon \cos \theta\right]^3} \quad .$$

Note that Equations 21 and 22 are not directly applicable for determining the normalized bearing inlet pressure in this case since constant radial clearance has been assumed in the development of these equations. For $\varepsilon = 0$, Equation 28 reduces to the constant radial clearance form, Equation 25.

In Figure 9 pressure profiles for a spherical bearing pad are presented at eccentricity ratios of 0.4 and 0.8. It was assumed that the bearing was machined with a constant radial clearance of $c = 0.0015$ inches. These pressure profiles are compared with pressure profiles that were derived assuming that the radial clearance was constant and equal to the average of the variable radial clearance. The dramatic effect of large eccentricity is clearly demonstrated in this figure.

Viscous inertial flow. At large film thicknesses or under conditions of high mass flow, inertia forces in the laminar gas film may become important ($Re^* \simeq 1$). Under these conditions the equations for gas lubrication developed in Appendix A are no longer valid. For the bearing configuration under consideration operating at these conditions the equations given in Appendix A which describe the flow reduce to:

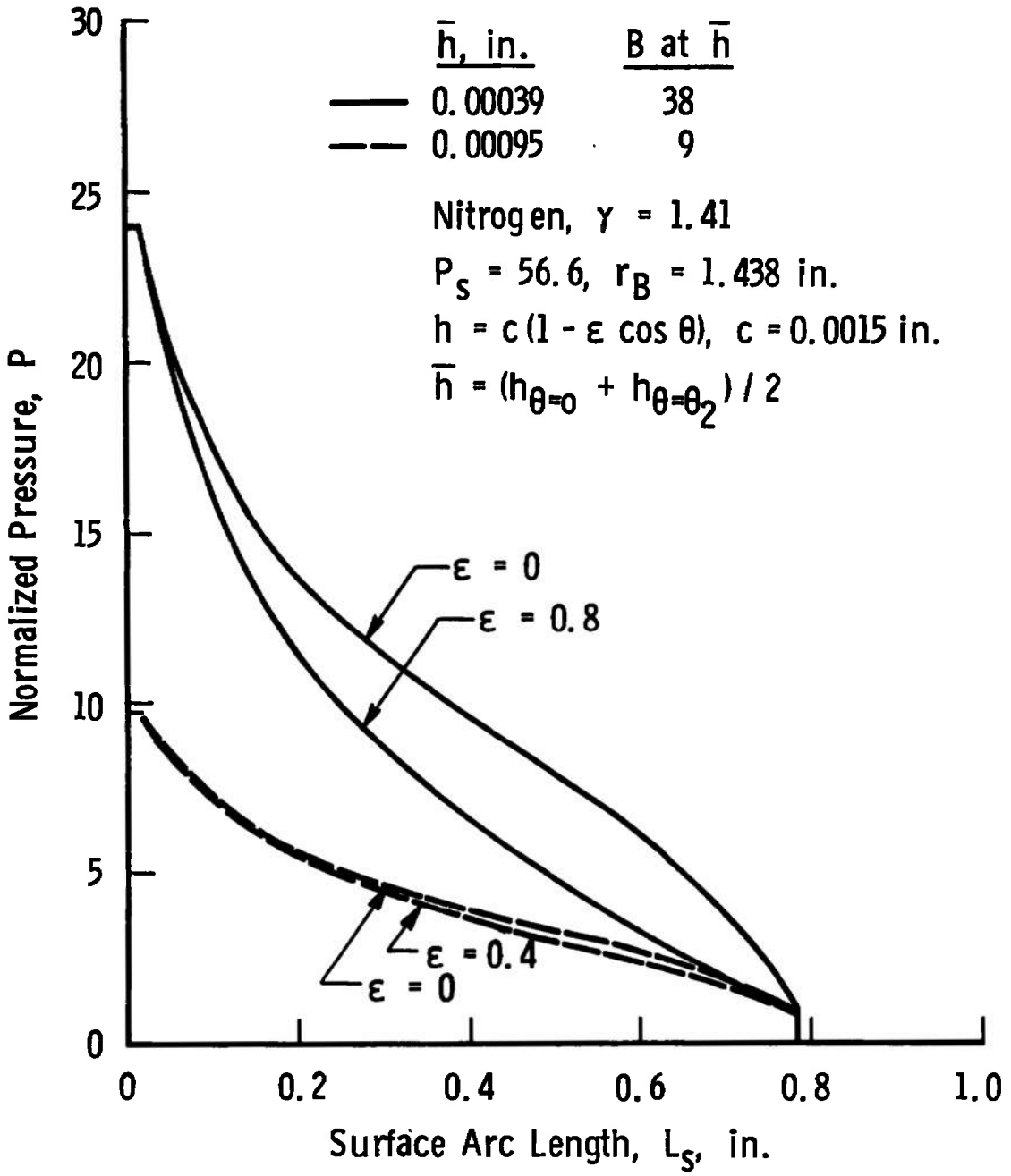

Figure 9. Pressure reduction due to eccentricity.

Momentum,

$$\rho \frac{u}{r} \frac{\partial u}{\partial \theta} + \frac{1}{r} \frac{\partial p}{\partial \theta} = \frac{\partial}{\partial z} \left[\mu \frac{\partial u}{\partial z} \right] ; \qquad (29)$$

Continuity,

$$\frac{\partial}{\partial \theta} (\rho u \sin \theta) = 0 ;$$

Energy,

$$\rho \frac{u}{r} \frac{\partial (c_p T)}{\partial \theta} = \frac{u}{r} \frac{\partial p}{\partial \theta} + \frac{1}{r^2} \frac{\partial}{\partial z} \left[r^2 k \frac{\partial T}{\partial z} \right] + \mu \left[\frac{\partial u}{\partial z} \right]^2 .$$

An exact solution for the pressure distribution of the film under these conditions would require numerical procedures since the above equations are coupled. Approximate analyses of this problem have been performed by many authors. Gross (3) and Comolet (14, 15) have obtained approximate solutions in cylindrical coordinates assuming that the film is polytropic and the velocity profile is parabolic. The last assumption requires that the inertia effects be small. This type analysis is easily adaptable to spherical coordinates; however, the effects of fluid inertia on the pressure

profile can be determined using Equation 29 without going through this lengthy process.

Rearranging Equation 29,

$$\frac{\partial p}{\partial \theta} = - \rho u \frac{\partial u}{\partial \theta} + r \frac{\partial}{\partial z}\left[\mu \frac{\partial u}{\partial z}\right].$$

For a parabolic velocity profile the last term on the right hand side of the above equation is negative (see Equation 14). In order that a lubricating film exist, it is necessary that $\partial p/\partial \theta < 0$. The larger $\partial p/\partial \theta$ is in absolute value, the greater the pressure produced by the film. Since $\partial u/\partial \theta < 0$, it is apparent that the inertia effects decrease the absolute value of the pressure gradient and, therefore, reduce the magnitude of the pressure produced by the film.

Inviscid supersonic flow. Sonic velocity can exist at the inlet to the lubricating film (16, 17, 18, 19), particularly for radial flows, when the mass flow or bearing clearance is large. Under these conditions the flow behaves as though it were expanding through a nozzle. At the proper conditions the flow will become supersonic which results in drastically reduced static pressure due to the large kinetic energy. A system of shock waves will occur followed by lower velocity and increased pressure. It is obvious that viscosity can only slightly affect the flow in the immediate

vicinity of the inlet; therefore, inviscid, viscous-inertial and viscous regions can exist in the film. The low pressure supersonic region and the loss in total pressure through the shock waves decrease the pressure produced by the film compared to the viscous predictions.

Mori (20) obtained a solution for the radial gas flow between two parallel disks by assuming that only a supersonic region and a viscous region exist. This solution has been confirmed experimentally.

V. LOAD CARRYING CAPACITY

The load carrying capacity of the model bearing (Figure 2, page 7) is defined here as the resultant film force which acts along the axis of symmetry of the pad to resist external loads placed on the bearing. For the bearing configuration under consideration the load carrying capacity is given as

$$w = \pi R_1^2 p_1 + \int_{\theta_1}^{\theta_2} \int_{o}^{2\pi} p r_B R \cos\theta \, d\varphi \, d\theta - \pi R_2^2 p_2 ,$$

where

$$R = r_B \sin\theta .$$

Factoring this expression and performing the first

integration, the normalized load carrying capacity is obtained in general form as

$$W = \left[\frac{\sin\theta_1}{\sin\theta_2}\right]^2 P_1 + \frac{2}{(\sin\theta_2)^2}\int_{\theta_1}^{\theta_2} P\sin\theta\cos\theta\, d\theta - 1 , \tag{30}$$

where

$$W = \frac{w}{\pi r_B^2 (\sin\theta_2)^2 p_2} .$$

A general expression for the load carrying capacity of the bearing is obtained by substituting Equation 28 into Equation 30

$$W = \left[\frac{\sin\theta_1}{\sin\theta_2}\right]^2 P_1 + \frac{2P_1}{(\sin\theta_2)^2} \quad x$$

$$\int_{\theta_1}^{\theta_2}\left[1 + \frac{\left[1 - P_1^2\right]\int_{\theta_1}^{\theta} G(\theta)\, d\theta}{P_1\int_{\theta_1}^{\theta_2} G(\theta)\, d\theta}\right]^{\frac{1}{2}} \sin\theta\cos\theta\, d\theta - 1 , \tag{31}$$

where

$$G(\theta) = \frac{1}{\sin\theta(1 - \varepsilon\cos\theta)^3} .$$

Substituting Equation 25 into Equation 30, or letting $\varepsilon = 0$ in Equation 31, an expression for the load carrying capacity of a bearing with constant radial clearance is obtained as

$$W = \left[\frac{\sin\theta_1}{\sin\theta_2}\right]^2 P_1 + \frac{2P_1}{(\sin\theta_2)^2} \quad x$$

$$\int_{\theta_1}^{\theta_2}\left[1 + \frac{\left[P_1^2 - 1\right]}{P_1^2 \ln\tau_1} \ln\left(\frac{\tau}{\tau_1}\right)\right]^{\frac{1}{2}} \sin\theta\cos\theta\, d\theta - 1 \,. \tag{32}$$

There are no closed form solutions for the integrals in Equations 31 and 32; therefore, numerical integration methods are required.

Equation 32 may be reduced to an approximate form which is similar to the form given in References (3) and (13) for the load carrying capacity of a flat circular pad. This approximate solution has a limited range of applicability. It involves numerical integration; however, the integrals are in a form for which tables of solutions exist in handbooks.

If it is assumed that θ_2 is small, then Equation 32 may be reduced to

$$W = \left[\frac{\theta_1}{\theta_2}\right]^2 P_1 + \frac{2P_1}{\theta_2^2}$$

$$\int_{\theta_1}^{\theta_2} \left[1 + \frac{\left[P_1^2 - 1\right]}{P_1^2 \ln\left(\frac{\theta_1}{\theta_2}\right)} \ln\left(\frac{\theta}{\theta_1}\right)\right]^{\frac{1}{2}} \theta \, d\theta - 1 \, .$$

Let

$$I = \frac{-2P_1^2 \ln\left(\frac{\theta_1}{\theta_2}\right)}{P_1^2 - 1} \, , \tag{33}$$

then

$$W = P_1\Theta_1^2 + 2P_1\int_{\Theta_1}^{1}\left[1 - \frac{2}{I} \ln\left(\frac{\Theta}{\Theta_1}\right)\right]^{\frac{1}{2}} \Theta \, d\Theta - 1 \, , \tag{34}$$

where

$$\Theta = \frac{\theta}{\theta_2} \, .$$

Now let

$$\frac{\xi}{\sqrt{I}} = \left[1 - \frac{2}{I} \ln\left(\frac{\Theta}{\Theta_1}\right)\right]^{\frac{1}{2}} \, , \tag{35}$$

then

$$\xi^2 = I - \ln\left(\frac{\Theta}{\Theta_1}\right)^2 .$$

Using the above equality as the exponent of e, then taking the square root and manipulating the expression algebraically

$$\Theta = \Theta_1 e^{\frac{I}{2}} e^{\frac{-\xi^2}{2}} . \tag{36}$$

Substitute this result and Equation 35 into Equation 34 to obtain

$$W = P_1\Theta_1^2 - \frac{2P_1\Theta_1^2 e^I}{\sqrt{I}} \int_{\xi_1}^{\xi_2} \xi^2 e^{-\xi^2} d\xi - 1 . \tag{37}$$

Applying the small angle assumption to Equation 25 and combining it with Equations 33 and 35 yields

$$\xi = \sqrt{I}\,\frac{P}{P_1} . \tag{38}$$

The limits of integration in Equation 37 are determined using this expression and the following boundary conditions:

at $\theta = \theta_1$, $\xi = \xi_1$, $P = P_1$, $\Theta = \Theta_1$,

at $\theta = \theta_2$, $\xi = \xi_2$, $P = 1$, $\Theta = 1$.

Reversing the limits of integration and integrating by parts Equation 37 becomes:

$$W = \frac{P_1^2 \Theta_1^2 e^I}{\sqrt{I}} \int_{\frac{\sqrt{I}}{P_1}}^{\sqrt{I}} e^{-\xi^2} \, d\xi \, . \tag{39}$$

This expression reduces to:

$$W = P_1 \Theta_1^2 e^I \sqrt{\frac{\pi}{4I}} \left\{ \operatorname{erf}\left(\sqrt{I}\right) - \operatorname{erf}\left(\frac{\sqrt{I}}{P_1}\right) \right\} . \tag{40}$$

Values of the error function in the above equation are found tabulated in many mathematical tables.

Figure 10 gives a comparison between the solutions obtained from Equations 32 and 40. Flat pad theory from Reference (13) is also presented. For this comparison the pad boundary radii (R_1 and R_2) were held constant; therefore, θ_2 was varied by changing the radius of curvature (r_B) of the bearing.

This figure shows the increased load carrying capacity of a spherically surfaced pad over a flat pad. Flat pad theory is shown to yield a better approximation to the

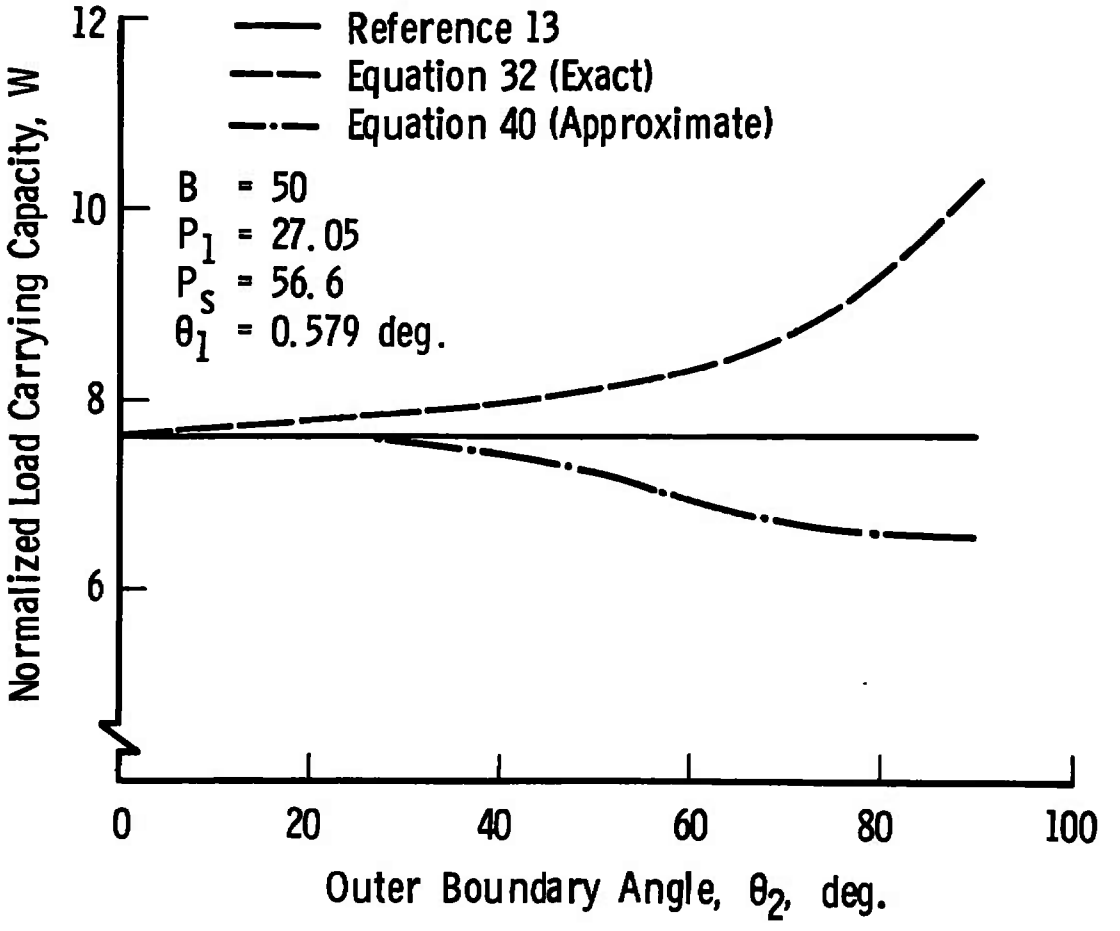

Figure 10. Comparison of various load capacity solutions.

results from Equation 32 than the simplified load carrying capacity theory of Equation 40. The simplified theory yields a 10 per cent error in load carrying capacity at $\theta_2 = 47.5$ degrees, while the flat pad theory yields this same error at $\theta_2 = 65$ degrees. The trend predicted by Equation 40 is opposite to that predicted by Equation 32.

For constant radial clearance

$$W = W(B, \tau_1, r_B, \gamma, P_S) .$$

Figure 11 shows that W increases continuously with B for constant γ and P_S. At the higher values of B this increase appears to become asymptotic. For a constant radius of curvature W increases with increasing B, τ_1, γ, and P_S. As discussed previously, the pad surface area is increased when the radius of curvature is decreased with the pad boundary radii being held constant. This results in decreased τ_1 and increased load capacity. Figure 10, page 43, shows that the load capacity for a fixed size pad is maximized when its geometry is hemispherical.

VI. STIFFNESS

The bearing stiffness is defined as the slope of the load carrying capacity versus radial clearance curve. For a hydrostatic bearing, operating with constant P_S and γ, it can be determined as follows:

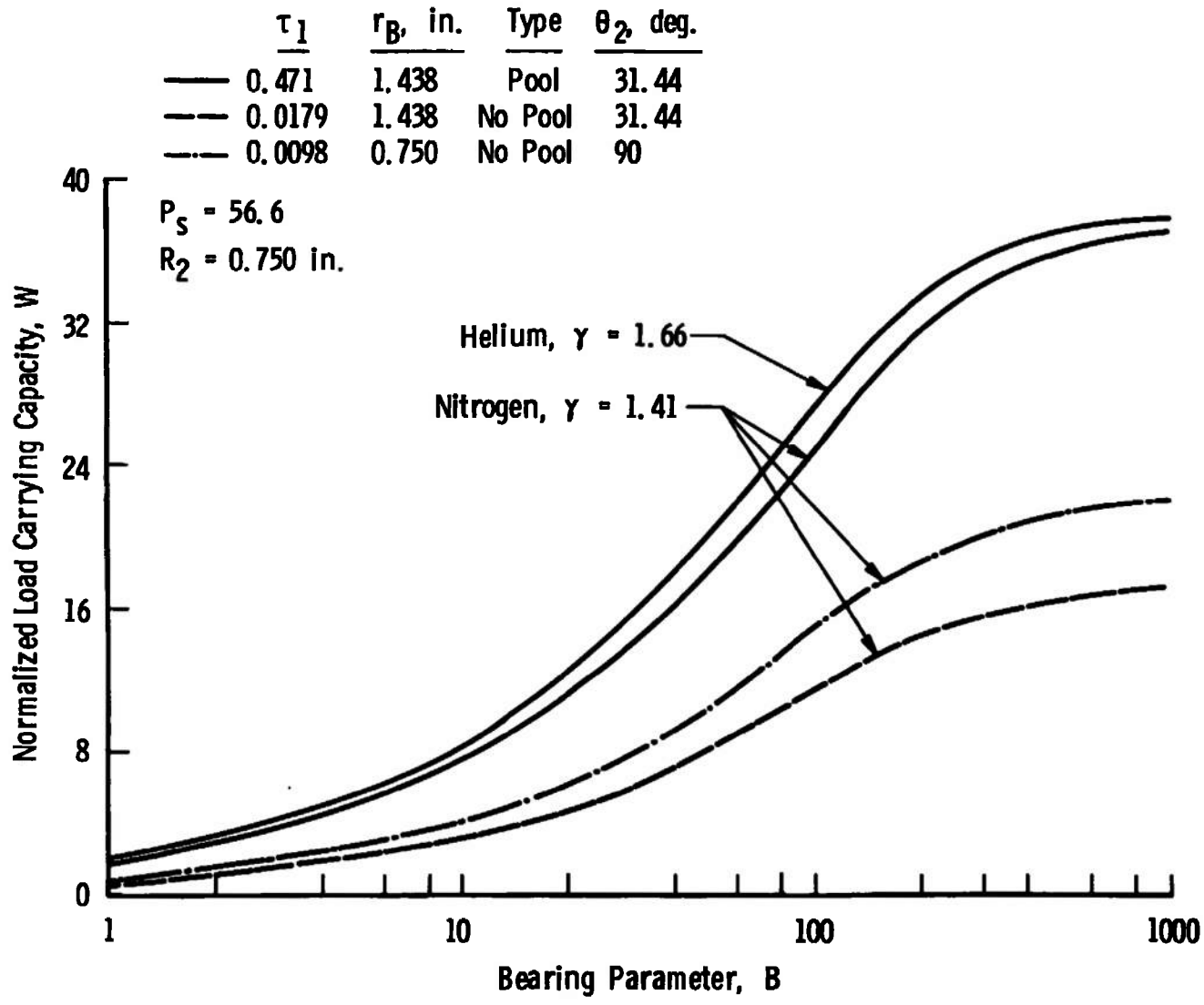

Figure 11. Theoretical load characteristics.

$$s = \frac{dw}{dh} = \frac{dw}{dP_1} \frac{dP_1}{dB} \frac{dB}{dh} . \qquad (41)$$

The stiffness is affected by the method of bearing compensation through the derivative dB/dh.

In order to evaluate the bearing stiffness, each of the derivatives in the above chain will be investigated separately. For any particular set of conditions these separate terms will be evaluated then substituted into Equation 41 to obtain the stiffness.

The derivative dw/dP_1. Differentiating Equation 32 with respect to P_1 yields dW/dP_1 for constant radial clearance

$$\frac{dW}{dP_1} = \left[\frac{\sin \theta_1}{\sin \theta_2}\right]^2 + \frac{2}{(\sin \theta_2)^2} \quad x$$

$$\int_{\theta_1}^{\theta_2} \left[1 + \frac{\left[P_1^2 - 1\right]}{P_1^2 \ln \tau_1} \ln\left(\frac{\tau}{\tau_1}\right)\right]^{\frac{1}{2}} \sin \theta \cos \theta \, d\theta$$

$$+ \frac{2}{P_1^2 (\sin \theta_2)^2 \ln \tau_1} \quad x$$

$$\int_{\theta_1}^{\theta_2} \frac{\ln\left(\frac{\tau}{\tau_1}\right) \sin\theta \cos\theta \, d\theta}{\left[1 + \frac{\left[P_1^2 - 1\right]}{P_1^2 \ln \tau_1} \ln\left(\frac{\tau}{\tau_1}\right)\right]^{\frac{1}{2}}} . \qquad (42)$$

Recall that

$$\frac{dw}{dP_1} = (\pi R_2^2 p_2) \frac{dW}{dP_1} .$$

There are no closed form solutions for the above integrals; therefore, numerical integration methods are once again required.

Equation 42 can be reduced to an approximate form which is similar to the form given in Reference (3) and (13) for the derivative dw/dP_1 of a flat circular pad. The range of applicability of this solution will be limited to the applicable range of Equation 40. The final result will require the evaluation of Equation 40 which is accomplished using numerical tables.

Assuming that θ_2 is small, using Equation 33 and the definition of Θ, Equation 41 can be reduced to

$$\frac{dW}{dP_1} = \Theta_1^2 + 2 \int_{\Theta_1}^{1} \left[1 - \frac{2}{I} \ln\left(\frac{\Theta}{\Theta_1}\right)\right]^{\frac{1}{2}} \Theta \, d\Theta -$$

$$\frac{2}{I\left[P_1^2 - 1\right]} \int_{\Theta_1}^{1} \left[1 - \frac{2}{I} \ln\left(\frac{\Theta}{\Theta_1}\right)\right]^{\frac{1}{2}} 2 \ln\left(\frac{\Theta}{\Theta_1}\right) \Theta \, d\Theta \, .$$

Substitute Equations 35 and 36 into this relation. Use Equation 38 and the boundary conditions on page 42 to determine the new limits of integration. After reversing the limits of integration this procedure results in

$$\frac{dW}{dP_1} = \Theta_1^2 + \frac{2P_1\Theta_1^2 e^I}{\sqrt{I}} \left[\frac{P_1}{P_1^2 - 1}\right] \int_{\frac{\sqrt{I}}{P_1}}^{\sqrt{I}} \xi^2 e^{-\xi^2} \, d\xi -$$

$$\frac{2P_1\Theta_1^2 e^I I}{\sqrt{I}} \left[\frac{P_1}{P_1^2 - 1}\right] \int_{\frac{\sqrt{I}}{P_1}}^{\sqrt{I}} e^{-\xi^2} \, d\xi \, .$$

Integrating the first integral by parts and recalling Equation 39

$$\frac{dW}{dP_1} = \frac{P_1}{P_1^2 - 1} \left\{ W\left[1 - \frac{2I}{P_1^2}\right] + 1 - \frac{\Theta_1^2}{P_1} \right\}, \qquad (43)$$

where W is obtained from Equation 40.

The derivative dP_1/dB. For the unchoked flow condition the bearing inlet pressure is given by Equation 21. This equation is more easily differentiated after it has been rearranged. The following forms of Equation 21 prove useful in obtaining the final expression of the derivative

$$P_1^2 - 1 = BP_S^{\frac{\gamma-1}{2\gamma}} P_1^{\frac{1}{\gamma}} \sqrt{P_S^{\frac{\gamma-1}{\gamma}} - P_1^{\frac{\gamma-1}{\gamma}}} \quad , \tag{21.1}$$

$$P_S^{\frac{\gamma-1}{\gamma}} - P_1^{\frac{\gamma-1}{\gamma}} = \frac{P_1^2 - 1}{BP_S^{\frac{\gamma-1}{2\gamma}} P_1^{\frac{1}{\gamma}}} \quad , \tag{21.2}$$

$$\frac{B^2 P_S^{\frac{\gamma-1}{\gamma}} P_1^{\frac{2}{\gamma}}}{\left[P_1^2 - 1\right]^2} = \frac{1}{P_S^{\frac{\gamma-1}{\gamma}} - P_1^{\frac{\gamma-1}{\gamma}}} \quad . \tag{21.3}$$

Differentiate Equation 21.1 with respect to B and substitute Equation 21.2 into the result:

$$2P_1 \frac{dP_1}{dB} = \frac{\left[P_1^2 - 1\right]}{B} + \frac{\left[P_1^2 - 1\right]}{\gamma P_1} \frac{dP_1}{dB} -$$

$$\left[\frac{\gamma - 1}{2\gamma}\right] \frac{B^2 P_S^{\frac{\gamma-1}{\gamma}} P_1^{\frac{1}{\gamma}}}{\left[P_1^2 - 1\right]} \frac{dP_1}{dB} \quad .$$

Factoring this equation and substituting Equation 21.3 yields

$$\frac{dP_1}{dB} = \frac{\left[P_1^2 - 1\right]}{2P_1 B}\left\{1 - \frac{\left[P_1^2 - 1\right]}{2\gamma P_1^2} \quad x \right.$$

$$\left.\left[1 + \frac{(\gamma - 1)}{2}\,\frac{1}{\left(1 - \left[\frac{P_S}{P_1}\right]^{\frac{\gamma-1}{\gamma}}\right)}\right]\right\}^{-1} . \qquad (44)$$

This gives the derivative when the flow is not choked.

For the choked flow condition, Equation 22 gives the bearing inlet pressure. This equation is operated on and rearranged to obtain the following useful relations:

$$P_1^2 - 1 = BP_S P_c^{\frac{1}{\gamma}} \sqrt{1 - P_c^{\frac{\gamma-1}{\gamma}}} \quad , \qquad (22.1)$$

$$\sqrt{1 - P_c^{\frac{\gamma-1}{\gamma}}} = \frac{\left[P_1^2 - 1\right]}{BP_S P_c^{\frac{1}{\gamma}}} \quad . \qquad (22.2)$$

Differentiating Equation 22.1 with respect to B and substituting Equation 22.2

$$\frac{dP_1}{dB} = \frac{P_1^2 - 1}{2P_1 B} \quad . \qquad (45)$$

This gives the derivative when the flow is choked.

The derivative dB/dh. The bearing parameter is given in Equation 20. Only the term A_R/h^3 in this equation is a function of h. The method of bearing compensation determines the manner in which this term varies with h; therefore, the derivative dB/dh is dependent on the method of bearing compensation.

For the inherently compensated bearing with a pool, case 1b on page 13,

$$\frac{A_R}{h^3} = \frac{\pi d\left[h + \delta\right]}{h^3} .$$

Substituting this into Equation 20 and differentiating with respect to h,

$$\frac{dB}{dh} = \frac{-3B}{h}\left[1 - \left(\frac{1}{3}\right)\frac{1}{\left(1 + \frac{\delta}{h}\right)}\right] . \qquad (46)$$

For an inherently compensated bearing without a pool, case 2b on page 16,

$$\frac{A_R}{h^3} = \frac{\pi d}{h^2} ,$$

$$\frac{dB}{dh} = \frac{-2B}{h} . \qquad (47)$$

The final case in an orifice compensated bearing without a pool, case 2a on page 16,

$$\frac{A_R}{h^3} = \frac{\pi d_o^2}{4h^3} ,$$

$$\frac{dB}{dh} = \frac{-3B}{h} . \tag{48}$$

The effect of the restrictor on bearing stiffness is demonstrated by forming the ratio of Equation 47 and 48:

$$\frac{\left(\frac{dB}{dh}\right)_{Inherent}}{\left(\frac{dB}{dh}\right)_{Orifice}} = \frac{\frac{-2B}{h}}{\frac{-3B}{h}} = \frac{2}{3} .$$

This ratio shows that the inherent compensated bearing has only two thirds the stiffness of the orifice compensated bearing.

For constant radial clearance

$$S = S(B, \tau_1, r_B, \gamma, P_S) .$$

In addition, as demonstrated above, stiffness also depends on the method of bearing compensation. The theoretical information presented in Figure 12 was obtained for the spherical model bearing (R_2 = 0.75 inches and r_B = 1.438

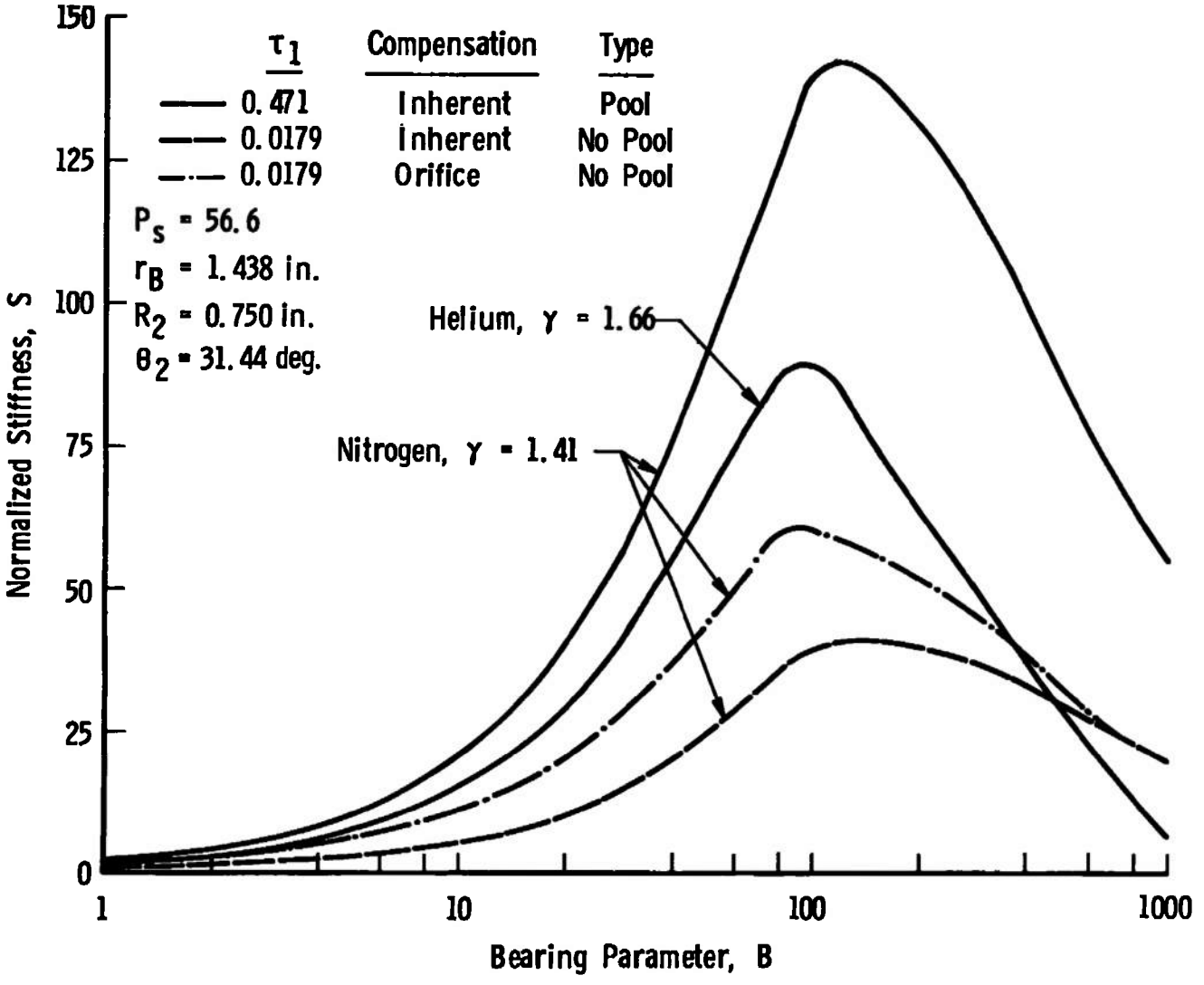

Figure 12. Theoretical stiffness characteristics.

inches). This figure demonstrates that with γ, r_B, τ_1, and P_S constant the stiffness increases with B until it reaches a maximum, then decreases with increasing B. It is important to note that with B, r_B, τ_1, and P_S held constant, increasing γ decreases the stiffness level. The small increase in γ caused a considerable reduction in the maximum stiffness level. Although not shown, the trends of stiffness with r_B, τ_1, and P_S will be similar to the trends of the load carrying capacity with these same variables. For a given configuration, as predicted above, orifice compensation is shown to increase the stiffness level over that obtained using inherent compensation by a factor of 1.5.

CHAPTER IV

EXPERIMENTAL TECHNIQUE

I. • PROCEDURE

An experimental investigation was conducted to verify theoretical predictions of the static and dynamic characteristics of the model bearing for different restrictor configurations. The parameters which were varied in this investigation are given as follows:

1. Supply pressure (p_s),
2. Bearing load (w),
3. Pool depth (δ),
4. Restrictor type (inherent and orifice),
5. Gas type (nitrogen and helium), and
6. Restrictor size.

Model configurations used in these studies are given in Table I.

The object of this experimental investigation was to determine the actual load capacity of each configuration and to observe its dynamic behavior when nitrogen is used as the working gas. Helium was used only to obtain additional data from these configurations for theoretical comparison.

Bearing dynamic stability and load capacity were determined for a given configuration at a given load by

TABLE I

MODEL BEARING CONFIGURATIONS

Configuration	τ_1	d in.	d_o in.	δ in.	θ_1 rad.	θ_2 rad.	Compensation
A	0.0179	0.029	0.029	0.0	0.01008	0.5488	Inherent
B	0.0179	0.029	0.005	0	0.01008	0.5488	Orifice
C	0.471	0.029	0.029	0.0005	0.2639	0.5488	Inherent
D	0.02902	0.047	0.047	0	0.01634	0.5488	Inherent
E	0.03458	0.055	0.055	0	0.01947	0.5488	Inherent
F	0.471	0.029	0.029	0.001	0.2639	0.5488	Inherent
G	0.471	0.029	0.029	0.002	0.2639	0.5488	Inherent
H	0.471	0.039	0.039	0.0005	0.2639	0.5488	Inherent

r_B = 1.438 in.

measuring the bearing deflection at supply pressures ranging from approximately 850 psig down to the pressure at which either air hammer instability resulted or the film collapsed. This was usually done in 50 psi steps. A complete list of the experiments which were conducted is given in Table II.

II. PRECISION OF RESULTS

The accuracies of both the bearing deflection measurements and the physical dimensions of each bearing configuration were of primary concern. In order to improve the accuracy of the deflection measurements, both the dial indicator calibration and alignment were checked periodically. When configuration changes were made, the bearing was set up in the shop and adjusted until the dimensions given in Table I, page 56, were assured. This adjustment quite often involved re-lapping the bearing surfaces. Estimates of the accuracy of the quantities measured in this investigation are given in Table III, page 59.

TABLE II

LIST OF EXPERIMENTS

Configuration	Load Range lb.	Load Increment lb.	Gas
A	25 - 225	25	N_2
A	50 - 200	50	He
B	25 - 225	25	N_2
B	25 - 275	50	He
C	25 - 250	25	N_2
C	75 - 225	150	He
D	25 - 250	25	N_2
E	25 - 250	25	N_2
F	25 - 50	25	N_2
F	25 - 50	25	He
G	25	25	N_2
G	25	25	He
H	25 - 75	25	N_2

TABLE III

DATA PRECISION

Measurement	Magnitude of Measurement	Estimated Error
d, d_o	0.005 to 0.055 in.	±0.0001 in.
h	0 to 0.003 in.	±0.00003 in.
p	0 to 850 psig	±2.5 psi
w	25 to 275 lb.	±0.2 lb.
δ	0.0005 to 0.002 in.	-0.0001 in.

CHAPTER V

RESULTS AND DISCUSSION

The object of this study was to determine a restrictor configuration which would maximize the load capacity and stiffness of the journal bearing while insuring pneumatic stability. It was also considered desirable to minimize the mass flow; however, this was a secondary consideration. Laminar restrictors were eliminated from consideration since they are known to be more susceptible to pneumatic instability and provide less stiffness than orifice type restrictors (10). Preliminary tests using the model bearing indicated that slight pneumatic instabilities existed with inherent compensation even at the smallest available pool volume. An orifice compensated pool type bearing was therefore not considered since its characteristics would tend to increase the possibility of pneumatic instability. The restrictor configurations considered were, therefore, inherent compensating both with and without a pool and orifice compensating without a pool.

I. STATIC CHARACTERISTICS

The journal bearing shown in Figure 1, page 2, should have been constructed such that each pad is operating at its

maximum stiffness level when there is no external load on the bearing. Under this condition the bearing will undergo a minimum deflection from its zero load position to compensate for a change in external load. This can be pictured with the aid of the single pad load characteristics presented in Figure 13 if the journal bearing is thought of as consisting of two horizontally opposed spherical thrust pads. The load carrying capacity of a simplified journal bearing of this type is obtained from a pad characteristic curve by taking the difference in the loads at the smaller and larger clearances of the deflected journal bearing. The difference in these clearances is indicated in Figure 13 as ΔH, which is the operating range of the journal bearing. The zero load constant radial clearance of the journal bearing is given as C.

In this figure characteristic curve 1 has its maximum stiffness point located at a clearance smaller than the zero load clearance, while characteristic curve 2 has its maximum stiffness point located at the zero load position. It is shown in this figure that in order to produce the same load carrying capacity a journal bearing operating with characteristic 1 must undergo a much greater deflection than one operating with characteristic 2.

The load characteristic curves shown in Figure 13, are for constant radial clearance. In a journal bearing the

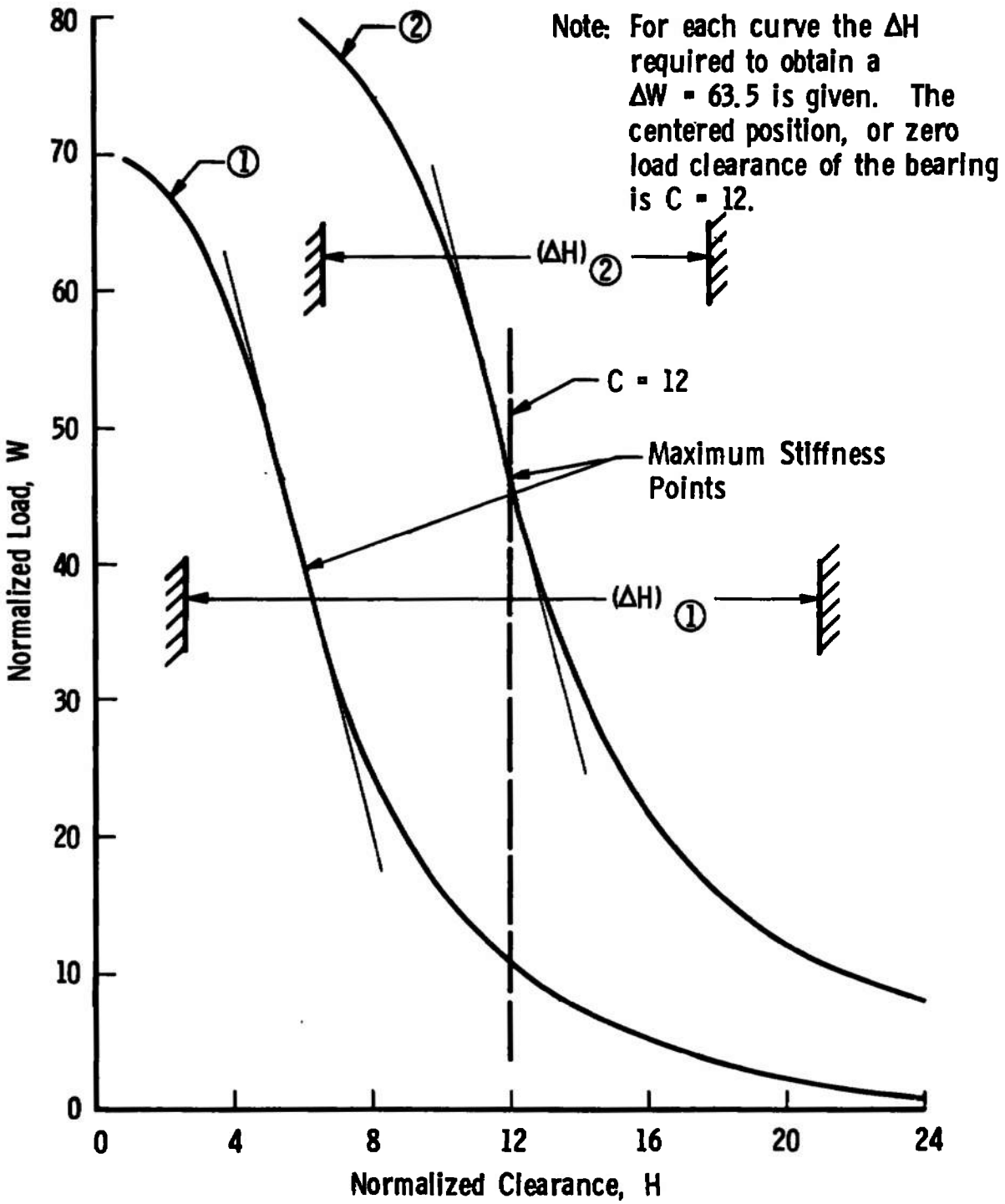

Figure 13. A comparison of pad load capacity characteristics.

radial clearance is constant only at the zero load position. As the bearing deflects from this centered position the absolute magnitude of the eccentricity ratio increases. The most important effects of eccentricity on film pressure are encountered at large positive eccentricity ratios. At this condition, as shown in Figure 9, page 34, the film pressure distribution is substantially reduced below that predicted by the constant radial clearance theory; therefore, the load carrying capacity is also reduced. For a given load capacity the absolute magnitudes of the eccentricity ratios experienced using characteristic curve 2 will be smaller than those experienced using characteristic 1; thus, characteristic curve 2 is once again more desirable.

The journal bearing shown in Figure 1, page 2, represents a configuration whose pads may not be operated at maximum stiffness when the bearing is in the zero load condition. It is shown in Figure 12, page 53, that when the pads are operated at $P_S = 56.6$ the maximum stiffness level for all restrictor configurations under consideration occurs at a bearing parameter somewhere in the range from approximately 90 to 140. Using the definition of the bearing parameter (Equation 20) it can be shown that for the 0.0015 inches zero load constant clearance of the existing journal bearing, and a bearing parameter in the above range, the restrictors under consideration will be of extremely large size. In all

cases they will produce values of Re^* which exceed the limits of the viscous-isothermal theory (see Appendix A). For the pool bearing configuration geometrical restraints would make it impossible to achieve the required restrictor size.

Increasing the pad size and decreasing the zero load constant radial clearance, would seem to be the direction to take in order to improve this situation. Unfortunately, due to angular freedom requirements on the bearing and the requirement that the bearing be self centering, no substantial increase in pad area is possible. By reducing the zero load constant radial clearance of the journal bearing so that $Re^* \ll 1$ for bearing parameters in the range 90 to 140, the optimum characteristic could be attained; however, the extremely small clearances at which the bearing would be required to operate invalidate this approach.

In attempting to obtain an optimum bearing restrictor for the journal bearing, it became obvious that in order to avoid the load capacity reduction resulting from viscous inertial flow, it would be necessary to use small restrictor sizes. Even for these small restrictors, the use of large supply pressures cast doubt on the validity of using viscous theory to describe the complete gas film. This is due to the increased possibility of supersonic flow at the inlet to

the film. These conditions made an experimental verification of the theoretical results a necessity.

In order to compare theoretically the performance of the various restrictor configurations being considered, d was fixed at 0.029 inches and estimates of bearing load carrying capacity, bearing stiffness, and bearing mass flow were obtained. These results for Configurations A, B, and C (see Table I, page 56) are presented in Figures 14, 15, and 16 where each value of h is assumed to represent a constant radial clearance and the supply pressure is held constant. For a restrictor of this size, Figure 15 shows that the pads would be operating well below maximum stiffness at the zero load position (h = 0.0015 inches). As related previously, this situation requires large bearing deflections to obtain maximum load capacity. The maximum practical journal bearing operating range is indicated in these figures and in many to follow.

These theoretical results indicate that for a journal bearing having the indicated operating range, the inherently compensated pool bearing (Configuration C) has the most desirable load capacity and stiffness characteristics, while the inherently compensated bearing without a pool (Configuration A) has the least desirable. The mass flow through the bearing would be minimized using orifice compensation

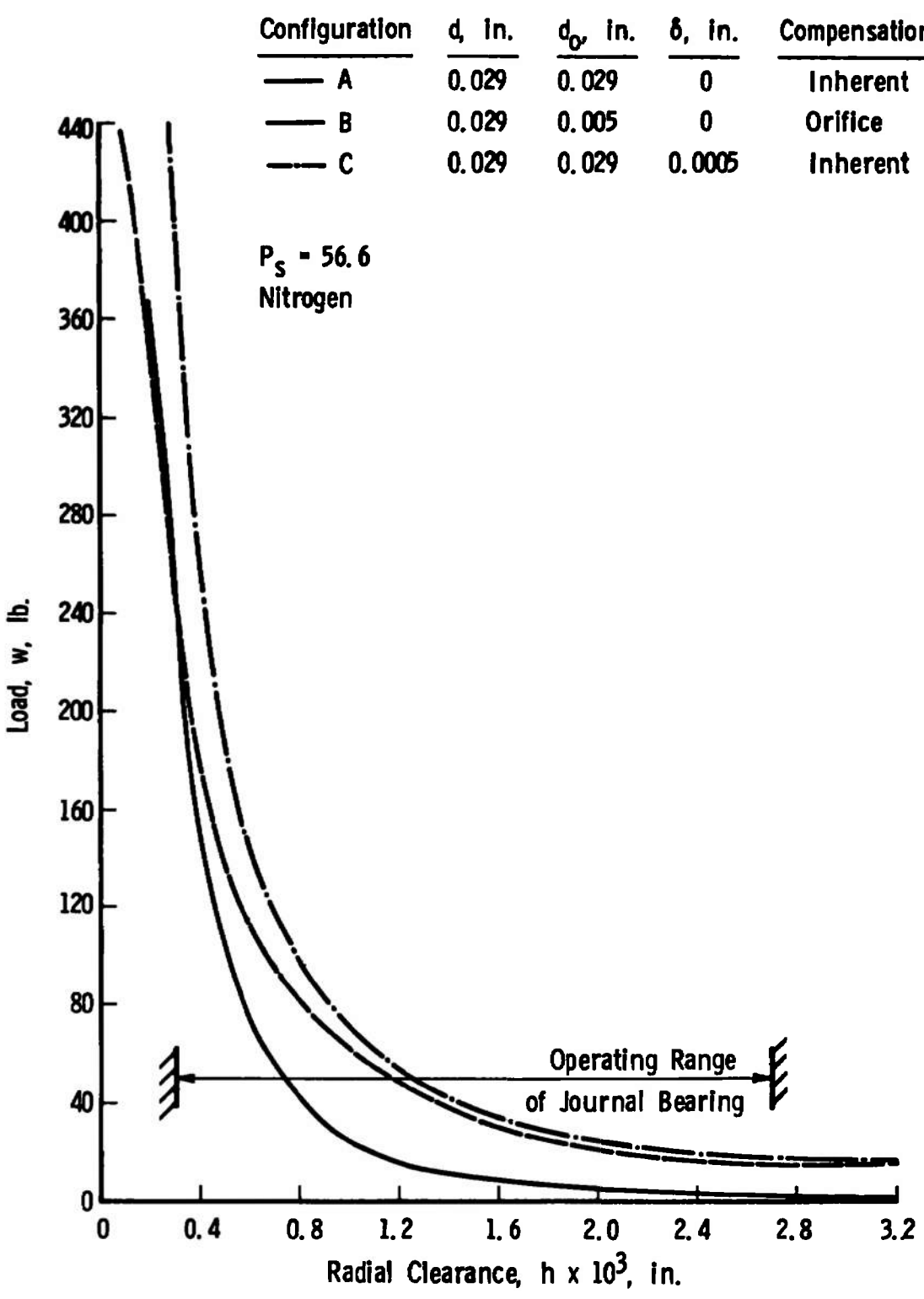

Figure 14. Theoretical pad load characteristics.

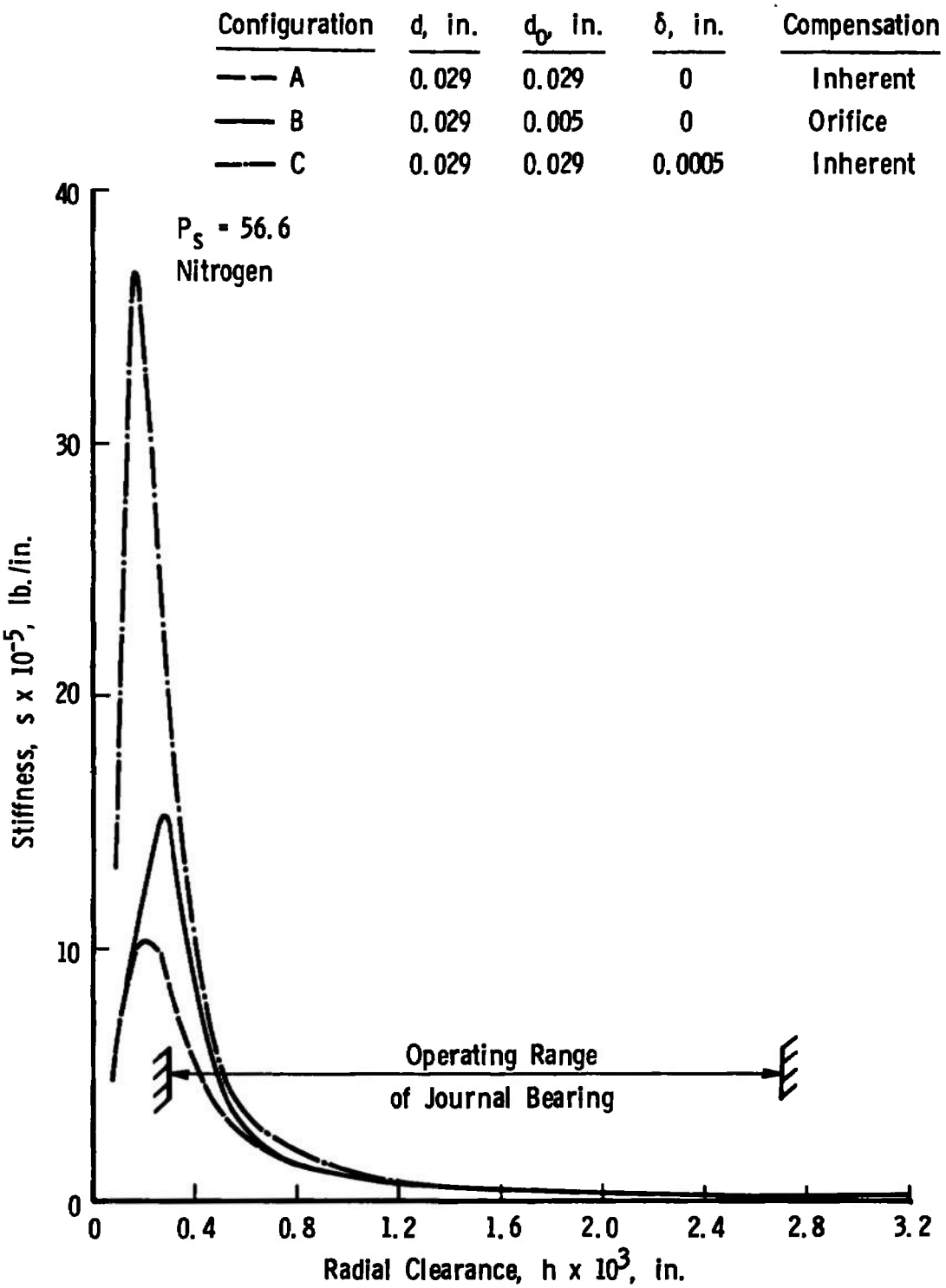

Figure 15. Theoretical pad stiffness characteristics.

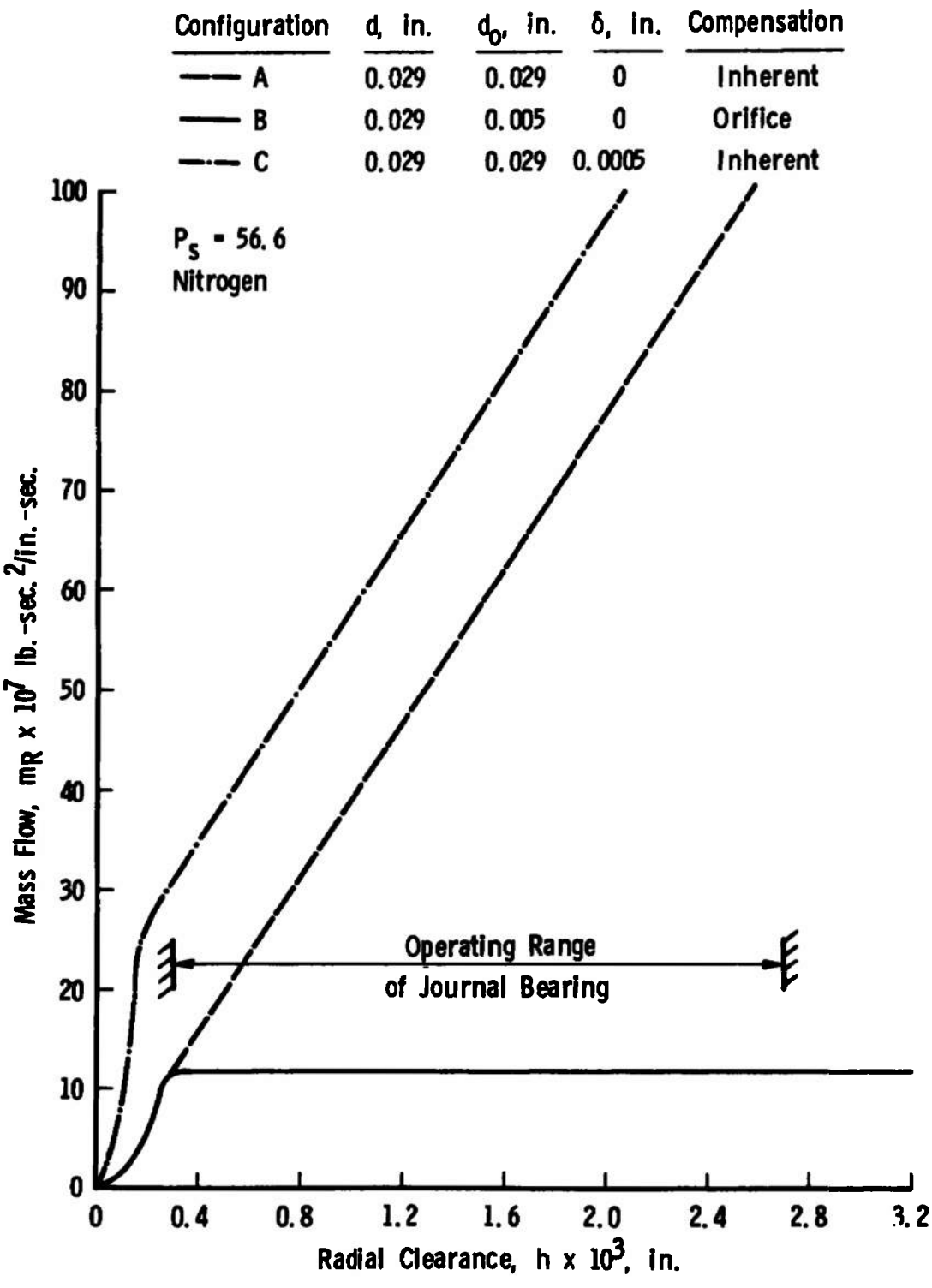

Figure 16. Theoretical pad mass flow characteristics.

(Configuration B). Maximum bearing mass flow would be obtained when inherent compensation with a pool is employed.

It should be noted here again that these theoretical results do not account for the pressure recovery in the flow after it leaves the restrictor. In the theoretical development, it has been assumed that all of the kinetic energy imparted to the flow as it leaves the restrictor is dissipated. Therefore, the film inlet pressure must be the static pressure downstream of the restrictor at the vena contracta. Some of the kinetic energy is recovered as pressure; thereby, making the actual inlet pressure higher than the predicted value. Naturally, the greater the pressure differential across the restrictor the larger the kinetic energy. As shown by Vohr (10), this has the effect of increasing the mass flow and decreasing the stiffness when compared to the theoretical predictions. Vohr has observed, as one might expect, that the pressure recovery for inherent compensation is greater than that for orifice compensation.

An experimental investigation was conducted to verify the theoretical bearing load carrying capacity estimates for model bearing Configurations A, B, and C. Results from this investigation obtained at a constant supply pressure are presented in Figures 17, 18, and 19. As predicted by the viscous-isothermal theory, for a fixed supply pressure, the use of helium causes a considerable increase in pad load

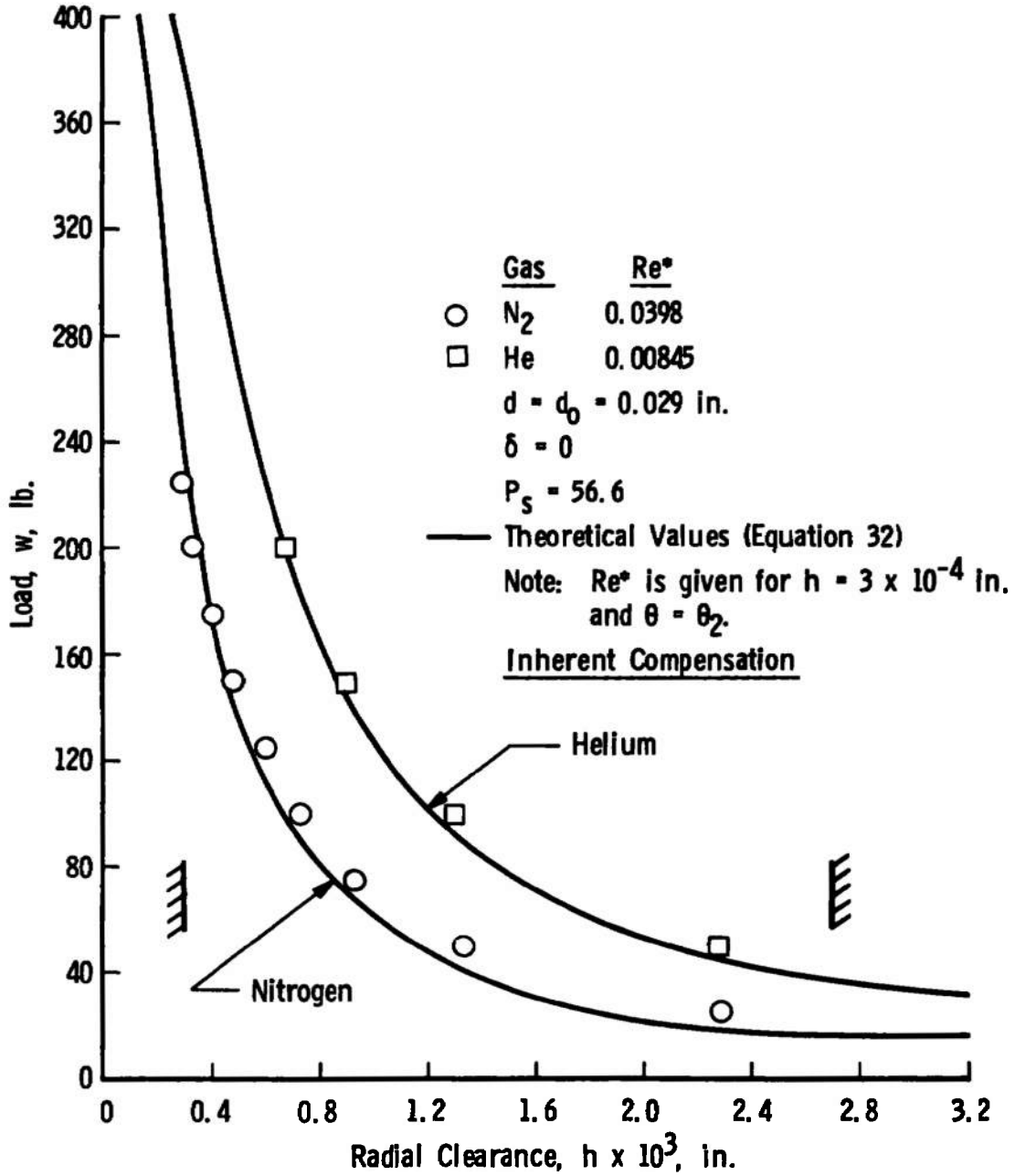

Figure 17. Experimentally determined load characteristics of Configuration A.

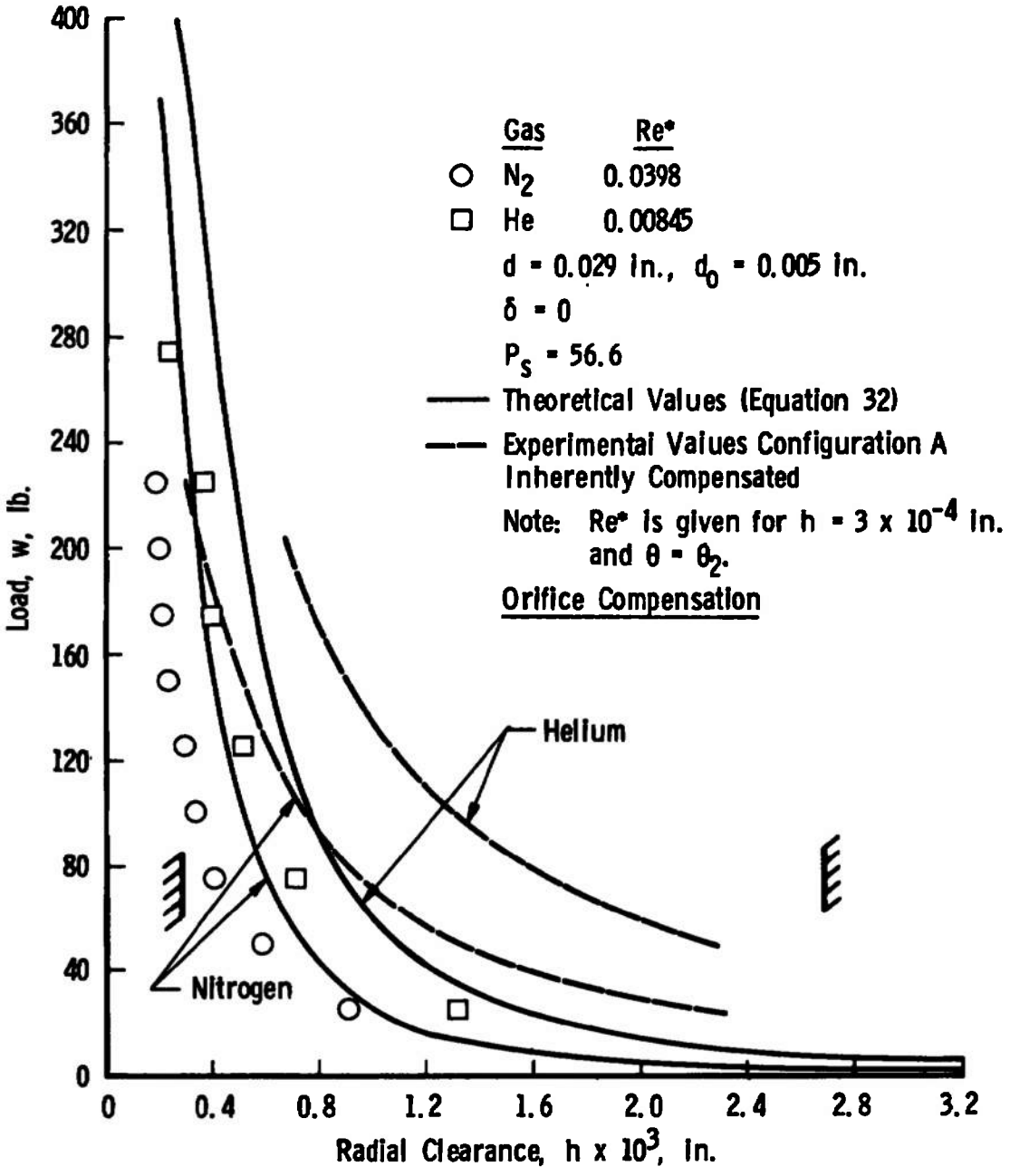

Figure 18. Experimentally determined load characteristics of Configuration B.

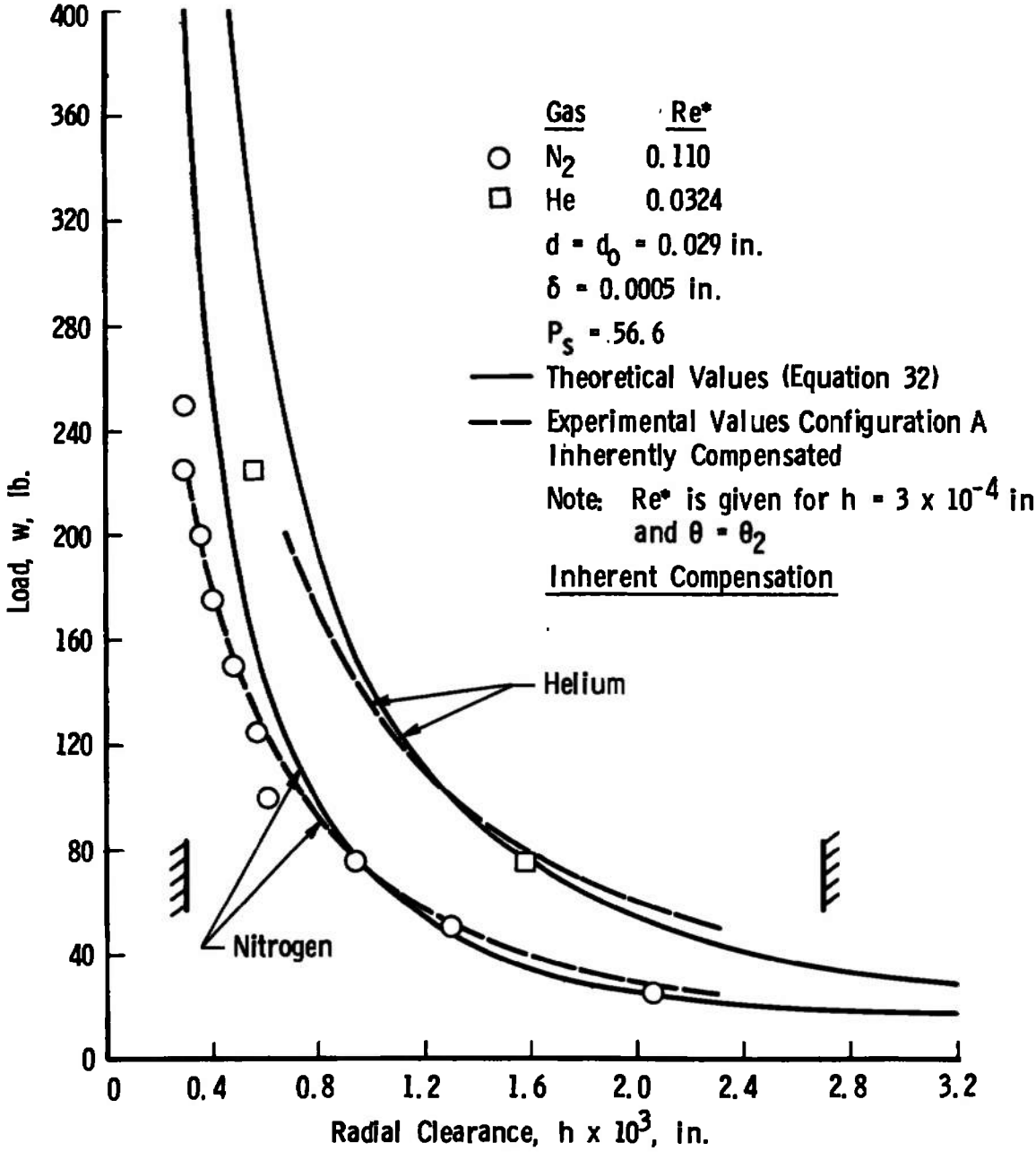

Figure 19. Experimentally determined load characteristics of Configuration C.

carrying capacity over that obtained using nitrogen. The primary reason for this great improvement in load carrying capacity is that at each particular value of the radial clearance the bearing parameter for helium is greater than that for nitrogen. Note that in all these figures, Re^* for helium is considerably smaller than that for nitrogen.

The load capacity theory used for comparison purposes in these figures was obtained from Equation 32 where constant radial clearance is assumed. This assumption should be valid for these comparisons since at the smaller radial clearances, which is the range of particular interest, the model bearing will be operating at small eccentricity ratios. This is a result of the method used in constructing the model bearing which has been discussed previously on page 6.

Given in Figures 17 and 18, pages 70 and 71, are the experimentally determined load carrying capacities of Configurations A and B. These results show that over the operating range of the simplified journal bearing the inherently compensated bearing is superior to the orifice compensated bearing. This is contrary to the theoretical comparison given in Figure 14, page 66, which predicts a slight advantage for the orifice compensated configuration. Note that the experimental data for Configuration A agree well with theoretical predictions while the experimental data for Configuration B do not.

The disagreement with theory for Configuration B is worse at radial clearances where it should be best. At the smaller radial clearances the effects of fluid inertia, pressure recovery, and eccentricity should be small. The performance of Configuration A substantiates this assumption. Since it appears that viscous-inertial flow is not directly responsible, the remaining inviscid effect likely at these values of Re^* is supersonic flow at the inlet to the film. It would then appear that at these particular operating conditions Configuration B suffers a greater pressure loss due to supersonic flow at the inlet than does Configuration A. As shown in Figure 4, page 14, the gas flow into the bearing film inlet for these restrictor configurations differs greatly.

The experimentally determined load capacity of Configuration C given in Figure 19, page 72, falls below the theoretical predictions. Due to the larger circumference of the film inlet section and the resulting reduced entrance velocities, the possibility of supersonic flow at the inlet should be remote. Viscous-inertial effects might be present particularly in the case of nitrogen due to the high values of Re^*; however, the resulting trends for helium are the same as those for nitrogen at one third the value of Re^*.

Experimental results for both nitrogen and helium seem to duplicate the experimental results for Configuration

A. This would seem to indicate either that a pool did not exist, or that the pressure in the pool is not constant as assumed theoretically. The fact that a pool effect existed can be established through Figure 20. Configuration C is shown to support the same load at a smaller supply pressure than Configuration A. Data obtained from Configuration F (see Table I, page 56) and presented in this figure indicate that increasing the pool depth above δ = 0.0005 inches will improve the load carrying capacity of the bearing. It would then seem that pool pressure for Configuration C is not constant as assumed. Configuration C offers no increase in load carrying capacity over Configuration A, which once again is contrary to the theoretical predictions.

The experimental results given in Figure 21, page 77, demonstrate the effect of bearing parameter (B) and modified Reynolds number (Re^*) on the load carrying capacity of the model bearing, when inherent compensation is used without a pool.

Theoretical trends given in this figure indicate that increased load carrying capacity may be obtained at a given radial clearance (h) by increasing the bearing parameter at that clearance. This procedure results in a shift of the load characteristic curve to the right, into a more favorable position. These theoretical results, of course, assume that the gas film is viscous dominated.

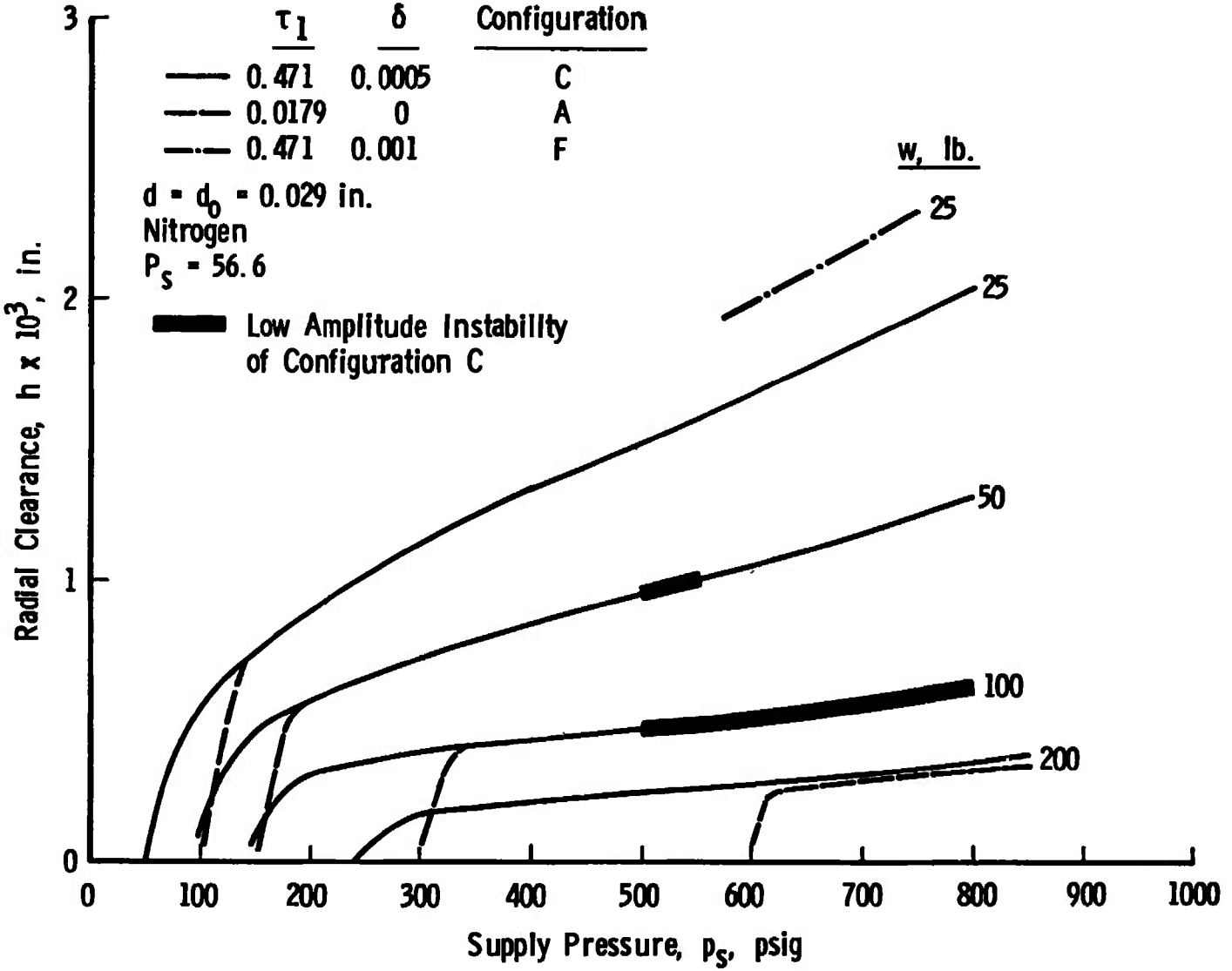

Figure 20. Effect of supply pressure on the load capacity of Configurations A and C.

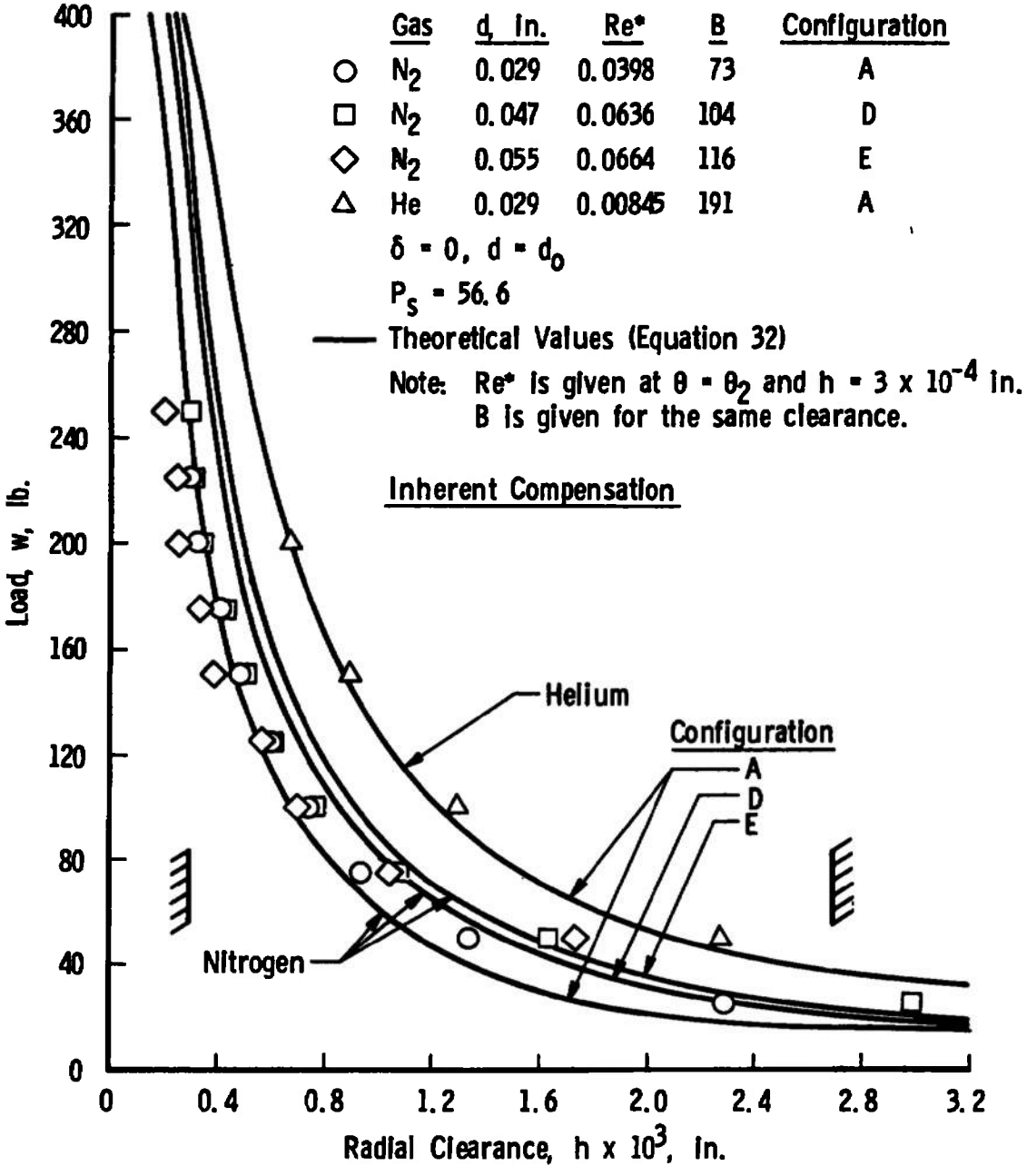

Figure 21. Effect of bearing parameter and Re* on the model bearing load carrying capacity.

The experimental results given for Configuration A in this figure conform to the above theoretical trends. The bearing parameter in this case was increased by changing the working gas from nitrogen to helium. This resulted in a decrease of Re^*.

When it becomes necessary to use a particular type gas, the bearing parameter may be increased by increasing the restrictor size. This method results in an increase of Re^*. Using this approach the experimental data for Configurations D and E (see Table I, page 56) were obtained. At the smaller radial clearances these data demonstrate a trend opposite to theoretical predictions. As the restrictor size increases, the load carrying capacity decreases. The increasing magnitude of Re^* indicates that inviscid effects in the film are responsible for these reversed trends. It would then appear that when nitrogen is used at this supply pressure Configuration A is approaching a limit for the viscous-isothermal theory.

This portion of the investigation has brought out many faults in the design of the existing journal bearing. These may be summed up as follows:

1. Pad areas too small,
2. Zero load constant radial clearance too large,
3. Operating range too large,
4. Load carrying capacity too small,

5. Operating pressure too high, and

6. Re^* too large.

There is nothing that can be done to this particular configuration which will substantially improve its performance. From the results of this investigation it would seem that the only practical modification would be to change the restrictor configuration to inherent compensating without a pool. If this proves to be unsatisfactory then the next step should be to design a new core.

II. DYNAMIC CHARACTERISTICS

Dynamic instabilities may be encountered in many bearing configurations, particularly journal bearings. When pressure pools are used, the chances of instability are increased. A gas bearing cannot be operated effectively when dynamic instabilities are present. The two most common types of dynamic instability encountered in gas journal bearings are pneumatic instability and whirl. Pneumatic instability is the subject of this investigation.

Whirl instability is inherent in many journal bearings. It occurs at continuous angular speeds above a certain critical speed. A bearing may, therefore, be operated at speeds below this critical value without encountering whirl. Increasing bearing film stiffness and decreasing effective

bearing mass both increase the magnitude of the critical speed.

As a result of fluid compressibility, the instantaneous mass inflow to the bearing does not in general equal the instantaneous mass outflow. Under the proper conditions this can supply a mechanism by which energy may be periodically added to the system in phase with the motion. This produces pneumatic instability or "air hammer," which is a dynamic instability independent of system resonances. Pneumatic instability is not as well ordered as whirl; therefore, it must be eliminated. Results from the experimental investigation presented herein, are for cases where this instability was encountered.

Due to the difficulty in establishing a complete analysis of this phenomena, approximate solutions have been obtained. In order to obtain these solutions, perturbation techniques have been used and it has been assumed that film entrance effects along with fluid acceleration and inertia forces are negligible. Using these assumptions the quasi-static lumped parameter analysis, References (4) through (8), and the distributed parameter analysis, Reference (9), have been obtained. The latter analysis includes density-time effects. The lumped parameter analysis neglects these effects and, therefore, does not include the damping due to squeeze film action.

Theoretical results given in these references indicate that the likelihood of pneumatic instability occurring is decreased by reducing the magnitude of the following:

1. Pool volume,
2. Pressure drop across the restrictor ($p_S - p_1$),
3. Bearing effective mass,
4. Bearing film stiffness (s), and
5. Heat transfer from the gas.

It is also decreased by increasing the magnitude of the following:

1. Supply orifice area (A_R),
2. Magnitude of the outer bearing limit (R_2) relative to the inner limit (R_1), and
3. Gas temperature.

Many of the trends listed above as having unfavorable effects on dynamic stability are considered desirable for improving static stability.

It should be noted that compared to orifice compensation, inherent compensation produces less stiffness and a smaller pressure drop across the restrictor. It does not require a pressure pool to operate. Richardson (5), using a lumped parameter analysis, has shown that the bearing damping is decreased by the existence of even the smallest pressure pool downstream of a restrictor. Increasing the bearing surface area of a gas bearing provides more squeeze

film surface and thus more damping. For these reasons, an inherently compensated bearing without a pool is theoretically the configuration least susceptible to pneumatic instability.

It was noted during this experimental investigation with the model bearing that in the majority of cases pneumatic instability began as a small disturbance at high pressures and grew in amplitude as the pressure was decreased. The limited ability to measure this instability, for this investigation, resulted in its development being grouped into the following three classifications:

1. Low amplitude instability. This stage in the development was detected by a high frequency noise. The amplitude was too small and the frequency too high to be measured by the dial indicator; however, when a sharp pointed instrument was placed against the bearing a vibration could be detected.
2. Measurable amplitude instability. This more developed stage was detected both by a high frequency noise and by an oscillation of the indicator needle.
3. Metal to metal instability (Air Hammer). The instability was completely developed at this stage and could be detected by the violent

unsymmetrical movement of the indicator needle and by the characteristic sound of metal surfaces in violent intermittent contact.

All of the instabilities noted during the experimental program are recorded in Figure 22. This figure used with Table II, page 58, will give complete information on the stability characteristics of the configurations which were tested. Figure 22 shows that the pool bearing configurations, with the exception of Configuration C, all encountered air hammer. The use of helium improved stability for these configurations. Slight instabilities were encountered with Configuration C. These instabilities appear in a somewhat random manner and are absent at the extremes of the load range. Configuration B exhibited instabilities over portions of its load range. These instabilities were generally larger than those encountered by Configuration C; however, air hammer did not result. This configuration had only a slight pool which was necessary to insure orifice compensation. It is of particular interest to note that all of the configurations tested demonstrated pneumatic instabilities with the exception of the inherently compensated configurations without a pool.

Figure 23, page 85, gives the experimentally determined stability characteristics of Configuration F. Changing the working gas from nitrogen to helium is shown to increase

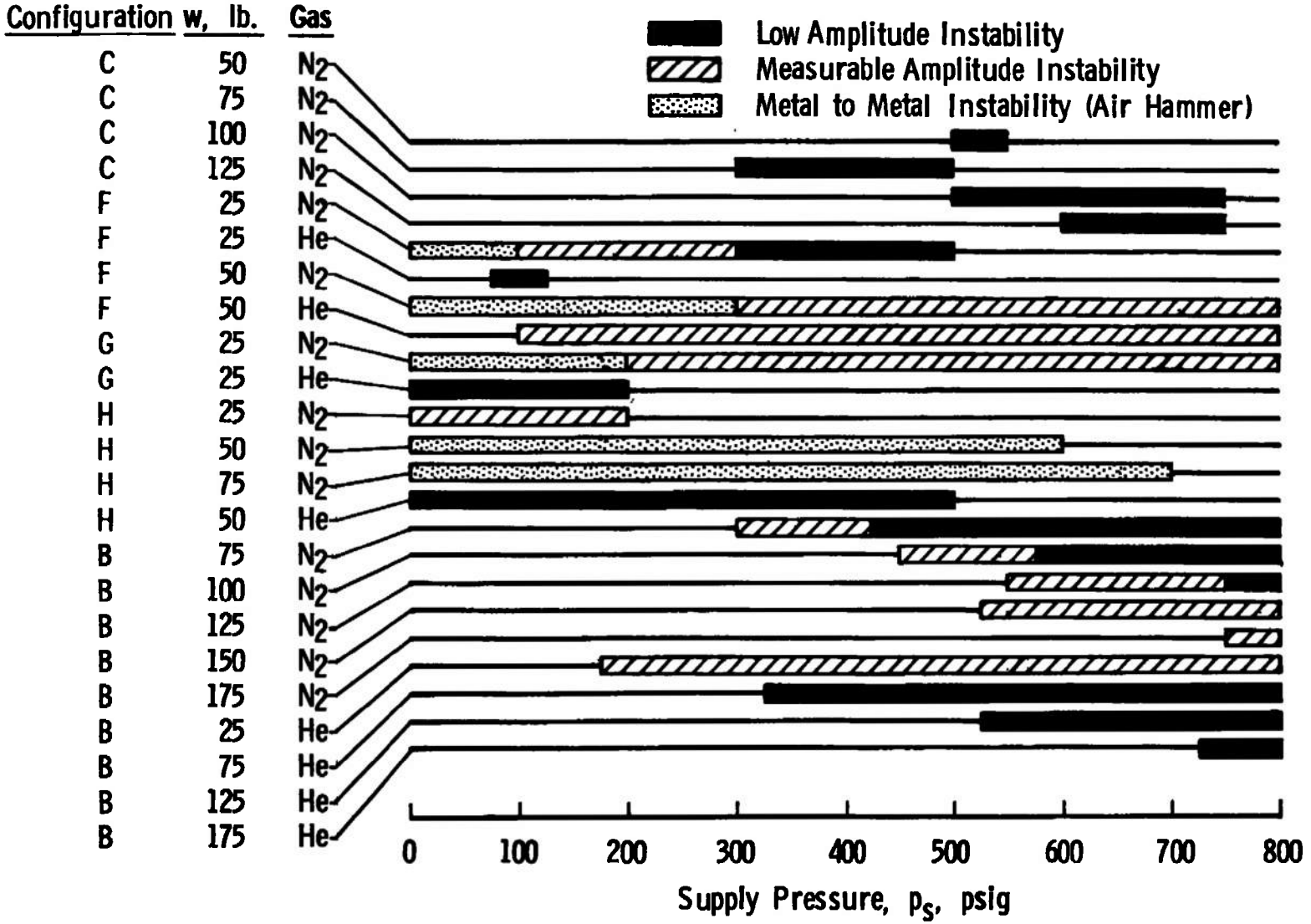

Figure 22. Summary of model bearing instabilities.

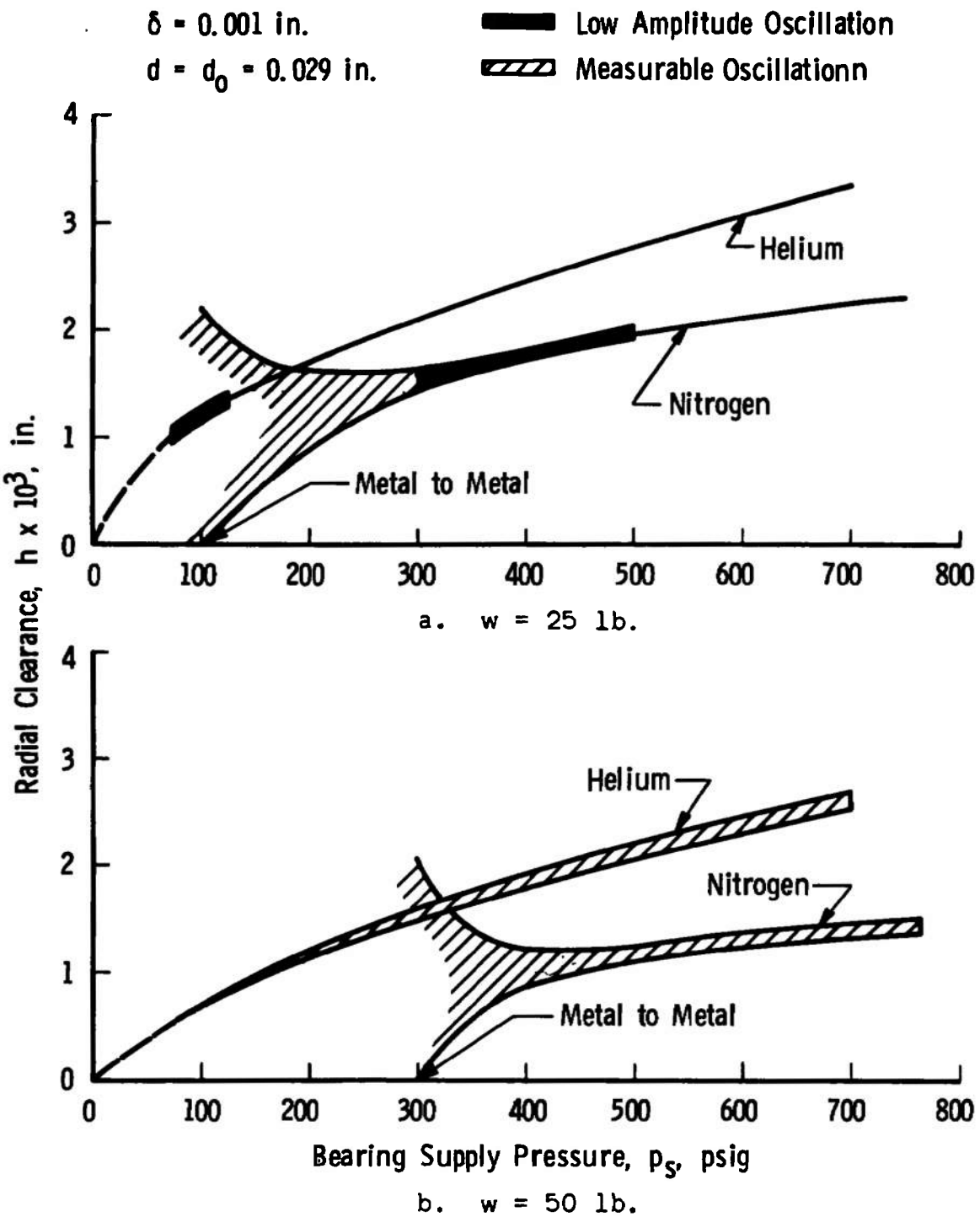

Figure 23. Dynamic instabilities of Configuration F.

stability. This has the effect of decreasing both the pressure drop across the restrictor and the stiffness. Increasing the load on the bearing is shown to decrease stability. This is a result of the increased effective mass. Comparing the results for Configuration F and those for Configurations C and G (see Table I, page 56) in Figure 22, page 84, it is shown that increasing the pool volume is destabilizing. All of the above trends are in agreement with theoretical predictions.

Comparing the performance of Configuration H (see Table I) with that of Configuration C, both given in Figure 22, it can be seen that increasing the restrictor size decreases stability. This is contrary to the theoretical predictions for a viscous dominated film; however, due to the high values of Re^* at the condition investigated it is highly doubtful that a viscous film existed. Due to the film conditions under which this instability was observed little can be said with certainty about its cause.

From the results of this portion of the investigation it is obvious that the pools of the journal bearing Figure 1, page 2, were much too large; thus, causing it to be unstable. Each pool was 14 times the size of the pool in Configuration F which was found to have a fully developed pneumatic instability.

The only restrictor configurations found to be completely stable during this investigation were the inherent restrictors without a pool. Fortunately the same type restrictors were also shown to be the best statically. The restrictor configuration of the journal bearing was changed to this type. The geometry of the modified journal bearing and its performance characteristics are presented in Appendix B.

CHAPTER VI

CONCLUSIONS

An investigation was conducted to determine a restrictor configuration which will insure pneumatic stability and maximize the load carrying capacity and stiffness of the pneumatically unstable spherical journal bearing shown in Figure 1, page 2. Restrictor configurations considered were inherent compensating both with and without a pool and orifice compensating without a pool. The model bearing shown in Figure 2, page 7, a duplicate of a journal bearing pad, was used for the experimental verification of theoretical predictions for the bearings static and dynamic characteristics.

Within the range of variables covered in the experimental investigation it can be concluded that changing the restrictor configuration of the existing journal bearing to inherent compensating without a pool will insure pneumatic stability and maximum load carrying capacity and stiffness. This conclusion is in agreement with theoretical predictions of dynamic behavior and is in disagreement with theoretical predictions of load carrying capacity and stiffness.

BIBLIOGRAPHY

1. Hodapp, A. E. "Evaluation of a Gas Bearing Pivot for a High Amplitude Dynamic Stability Balance," Arnold Engineering Development Center AEDC-TDR-62-221, Arnold Air Force Station, Tennessee, December, 1962.

2. Pan, C. H. T. "Spherical Hybird Bearing," Design of Gas Bearings, Vol. I, N. F. Reiger, editor. Latham, New York: Mechanical Technology Incorporated, 1966. Pp. 5.7.1-5.7.29.

3. Gross, W. A. Gas Film Lubrication. New York, London: John Wiley and Sons Incorporated, 1962.

4. Weber, R. R. "Investigation of Dynamic Response of Hydrodynamic Gas Bearings." Unpublished Master's thesis, The University of California at Los Angeles, Los Angeles, 1952.

5. Richardson, H. H. "Static and Dynamic Characteristics of Compensated Gas Bearings," Transactions of the American Society of Mechanical Engineers, 80:1503-1509, October, 1958.

6. Roudebusch, W. H. "An Analysis of the Effect of Several Parameters on the Stability of an Air Lubricated Hydrostatic Thrust Bearing," National Advisory Committee for Aeronautics Report TN 4095, Washington, D. C., 1958.

7. Licht, L., D. D. Fuller and B. Sternlicht. "Self Excited Vibrations of an Air Lubricated Thrust Bearing," Transactions of the American Society of Mechanical Engineers, 80:411-414, February, 1958.

8. Licht, L. "Axial Relative Motion of a Circular Step Bearing," Transactions of the American Society of Mechanical Engineers Journal of Basic Engineering, 81:109-117, June, 1959.

9. Licht, L. and H. Elrod. "A Study of the Stability of Externally Pressureized Gas Bearings," Transactions of the American Society of Mechanical Engineers Journal of Applied Mechanics, 82:250-258, June, 1960.

10. Vohr, J. H. "Restrictor Flows," Design of Gas Bearings, Vol. I, N. F. Reiger, editor. Latham, New York: Mechanical Technology Incorporated, 1966. Pp. 5.1.1-5.1.21.

11. Ames Research Staff. "Equations, Tables, and Charts for Compressible Flow," National Advisory Committee for Aeronautics Report 1135, Washington, D. C., 1953.

12. Vohr, J. H. "An Experimental Study of Flow Phenomena in the Feeding Region of an Externally Pressurized Gas Bearing," Mechanical Technology Incorporated Technical Report 65TR47, Latham, New York, 1966.

13. Tang, I. C. and W. A. Gross. "Analysis and Design of Externally Pressurized Gas Bearings," Transactions of the American Society of Lubrication Engineers, 5:261-284, April, 1962.

14. Comolet, Raymond. "Radial Flow of a Compressible Viscous Fluid Between Parallel Plates: Theoretical Study and Experimental Research on the Thrust Bearing," First International Symposium on Gas-Lubricated Bearings ACR-49, D. D. Fuller, editor. Washington, D. C.: United States Government Printing Office, 1959. Pp. 242-250.

15. Comolet, Raymond. "Ecoulement d'un fluide visqueux entre deux plans paralleles," Societe Francaise des Mecaniciens, 7:7-22, 1957.

16. Sasaki, T. and H. Mori. "On the Characteristics of Air Bearings," Koyoto University Faculty of Engineering Memoirs Volume 13 No. 1, Koyoto, Japan, 1951.

17. Ohno, T. and O. Taniguchi. "Research on the Air Thrust Bearing," Transactions of the Japan Society of Mechanical Engineers, 17:31-36, 1951.

18. Mueller, P. M. "Air Lubricated Bearings," Product Engineering, 22:112-115, August, 1951.

19. Deuker, E. A. and H. Wojtech. "Ecoulement radial d'un fliude visqueux entre deux disques tres reapproches. Theorie du palier a air," Revue generale de l'Hydraulique, No. 65, September-October, 1951, Pp. 227-234; No. 66, November-December, 1951, pp. 283-294.

20. Mori, Haruo. "A Theoretical Investigation of Pressure Depression in Externally Pressurized Gas-Lubricated Circular Thrust Bearings," Transactions of the American Society of Mechanical Engineers Journal of Basic Engineering, 83:201-208, June, 1961.

21. Huges, W. F. and E. W. Gaylord. Basic Equations of Engineering Science. New York: Schaum Publishing Company, 1964.

22. Grinnell, S. K. "Flow of a Compressible Fluid in a Thin Passage," Transactions of the American Society of Mechanical Engineers, 78: 765-771, May, 1956.

APPENDIXES

APPENDIX A

GAS LUBRICATION EQUATIONS

In this section the equations for the distributed film velocities and the Reynolds equation will be developed using spherical coordinates.[1] These equations form the foundation of the viscous theory for gas film lubrication. Figure 24 and the compressible forms given in Reference (21) for the Navier-Stokes momentum equations, the continuity equation and the energy equation are used in this development. In order to obtain analytical solutions for these nonlinear partial differential equations it becomes necessary to simplify their forms. This is accomplished in part by using the following assumptions which are characteristic of thin gas films:

1. The gas lubricating film is thin; i.e., $h/r_B \ll 1$.
2. Gradients in the r (or z) direction, are much greater than gradients in the θ or φ directions.
3. The component of velocity in the r (or z) direction is negligible compared to the components of velocity in the θ or φ directions ($w' \simeq 0$).

---

[1] The approach is similar to that used by Gross (3) for cartesian coordinates.

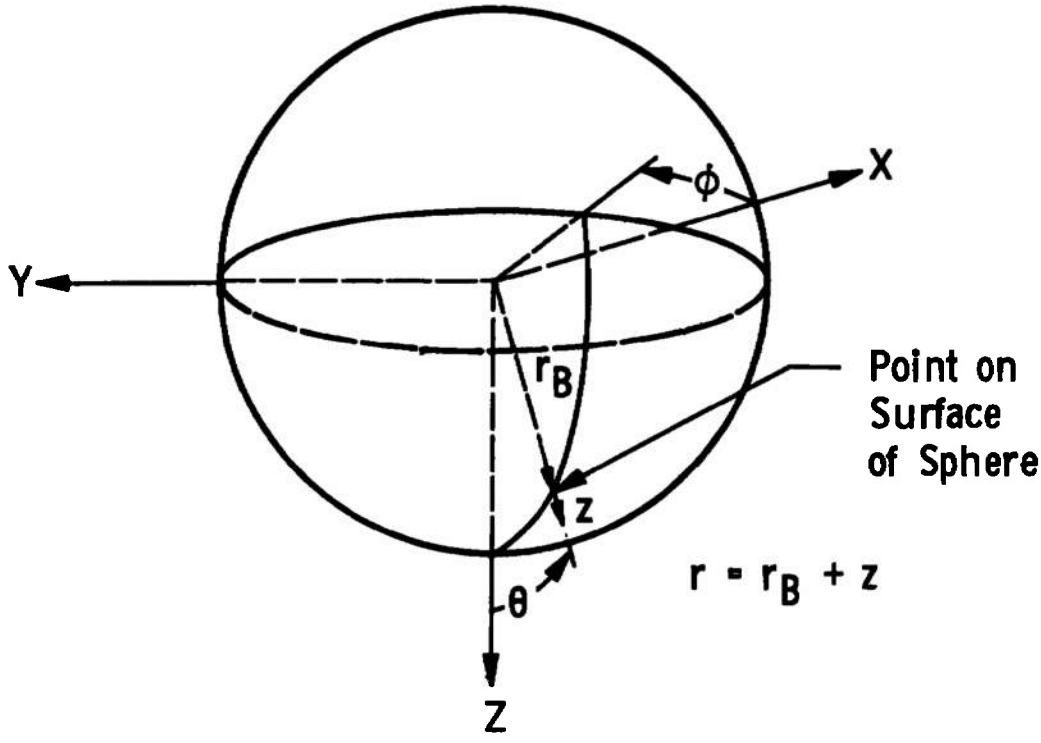

Figure 24. Coordinate system.

These assumptions along with the assumption of quasi-steady flow reduce the momentum and energy equations to the following forms:[2]

Momentum,

$$\rho\left[\frac{u}{r}\frac{\partial u}{\partial\theta} + \frac{v}{r\sin\theta}\frac{\partial u}{\partial\varphi} - \frac{v^2\cot\theta}{r}\right] + \frac{1}{r}\frac{\partial p}{\partial\theta} \simeq \frac{\partial}{\partial z}\left[\mu\frac{\partial u}{\partial z}\right], \tag{A-1}$$

$$\rho\left[\frac{u}{r}\frac{\partial v}{\partial\theta} + \frac{v}{r\sin\theta}\frac{\partial v}{\partial\varphi} + \frac{uv\cot\theta}{r}\right] + \frac{1}{r\sin\theta}\frac{\partial p}{\partial\varphi} \simeq \frac{\partial}{\partial z}\left[\mu\frac{\partial v}{\partial z}\right], \tag{A-2}$$

$$\frac{\partial p}{\partial z} \simeq 0 \; ; \tag{A-3}$$

Energy,

$$\rho\left[\frac{u}{r}\frac{\partial(c_pT)}{\partial\theta} + \frac{v}{r\sin\theta}\frac{\partial(c_pT)}{\partial\varphi}\right] =$$

---

[2]Note that the momentum equations and the energy equation are in the steady flow boundary layer form.

$$\frac{u}{r}\frac{\partial p}{\partial \theta} + \frac{v}{r \sin \theta}\frac{\partial p}{\partial \varphi} + \frac{1}{r^2}\frac{\partial}{\partial z}\left[r^2 k \frac{\partial T}{\partial z}\right] +$$

$$\mu\left[\left(\frac{\partial v}{\partial z}\right)^2 + \left(\frac{\partial u}{\partial z}\right)^2\right] ; \qquad \text{(A-4)}$$

where

$r = r_B + z$,

r_B = constant,

$r_B \gg h$, and

$0 \leq z \leq h$.

The continuity equation given in Reference (21) may be written as:

$$\frac{\partial \rho}{\partial t} + \frac{1}{r \sin \theta}\frac{\partial}{\partial \theta}(\rho u \sin \theta) + \frac{1}{r \sin \theta}\frac{\partial}{\partial \varphi}(\rho v)$$

$$+ \frac{1}{r^2}\frac{\partial}{\partial z}(r^2 \rho w') = 0 . \qquad \text{(A-5)}$$

Although the first and last terms in the above equation are negligible according to the assumptions used thus far, they have been retained so that the squeeze film effect will be included in the Reynolds equation. This effect is generally

small in the case of an externally pressurized bearing, but isolated conditions do exist under which it becomes important.

Equations A-1 and A-2 contain both viscous and inertial effects. Since only viscous effects are being considered, these equations may be reduced even further. The modified Reynolds number, Re^*, gives a good indication of the relative magnitudes of viscous and inertial forces in a gas film. It is an order of magnitude approximation of the ratio of interial force per unit volume to viscous force per unit volume which is defined here as:

$$\frac{\rho \dfrac{u}{r}\dfrac{\partial u}{\partial \theta}}{\mu \dfrac{\partial^2 u}{\partial z^2}} \simeq \frac{\dfrac{\rho \bar{u}^2}{r\theta}}{\dfrac{\mu \bar{u}}{h^2}} = \rho \frac{\bar{u} h^2}{\mu L_S} = \rho \frac{\bar{u} L_S}{\mu}\left[\frac{h}{L_S}\right]^2 =$$

$$Re^* ,$$

where $L_S = r\theta$ is the length of arc. When $Re^* \ll 1$, the inertial effects in the lubricating film become negligible when compared to the viscous effects and the momentum equations, Equations A-1 and A-2, reduce to:

$$\frac{1}{r}\frac{\partial p}{\partial \theta} = \frac{\partial}{\partial z}\left[\mu \frac{\partial u}{\partial z}\right], \qquad \text{(A-6)}$$

$$\frac{1}{r \sin \theta} \frac{\partial p}{\partial \varphi} = \frac{\partial}{\partial z}\left[\mu \frac{\partial v}{\partial z}\right] . \qquad \text{(A-7)}$$

Equations A-4, A-5, A-6, and A-7 are available for obtaining a solution to the problem. Add to this list the equation of state for a gas, which is

$$p = \rho RT , \qquad \text{(A-8)}$$

and the number of equations is increased to five.

In Equation A-3 it is shown that $p = p(\theta,\varphi)$. If the thermal gradient across the lubricating film $(\partial T/\partial z)$ is negligible then $\rho = \rho(\theta,\varphi)$. This is a valid assumption due to the low heat generating capacity of a gas film with $Re^* \ll 1$. The viscosity, μ, is known to be a function of temperature and to depend slightly on pressure; therefore, $\mu = \mu(\theta,\varphi)$.

The results of the previous discussion for a thin gas film with $Re^* \ll 1$ are:

$$\left.\begin{aligned} T &= T(\theta,\varphi), \\ p &= p(\theta,\varphi), \\ \rho &= \rho(\theta,\varphi), \\ \mu &= \mu(\theta,\varphi), \\ u &= u(\theta,\varphi,z), \text{ and} \\ v &= v(\theta,\varphi,z). \end{aligned}\right\} \qquad \text{(A-9)}$$

The boundary conditions for no slip at the gas boundaries are:

at $z = 0$, $u = 0$, $v = 0$, $w' = 0$;

at $z = h$, $u = u_h$, $v = v_h$, $w' = \dot{h}$.

Assuming that $r \simeq$ constant, since $r_B \gg z$, Equations A-6 and A-7 can be integrated with respect to z to obtain:

$$u = \frac{1}{2\mu r} \frac{\partial p}{\partial \theta} z\left[z - h\right] + u_h\left[\frac{z}{h}\right] , \qquad \text{(A-10)}$$

$$v = \frac{1}{2\mu r \sin \theta} \frac{\partial p}{\partial \varphi} z\left[z - h\right] + v_h\left[\frac{z}{h}\right] . \qquad \text{(A-11)}$$

The validity of these Poiseulle-Couette velocity profiles is dependent on the applicability of the Navier-Stokes equations; i.e., only in regions of small dilation. Since the conventional theory of lubrication is based on continuum flow with negligible slip and fluid inertia the region of applicability is further limited by:

$K_n < 0.01$,

$Re^* \ll 1$.

Transpose Equation A-5, the continuity equation, then integrate across the film in the z direction using the previous assumption that $r \simeq$ constant:

$$\frac{1}{r^2}\int_0^{(r^2\rho\dot{h})} d(r^2\rho w') = -\int_0^h \left[\frac{\partial\rho}{\partial t} + \right.$$

$$\left.\frac{1}{r\sin\theta}\frac{\partial}{\partial\theta}(\rho u\sin\theta) + \frac{1}{r\sin\theta}\frac{\partial}{\partial\varphi}(\rho v)\right]dz.$$

Interchanging integration and differentiation:

$$\frac{1}{r^2}\int_0^{(r^2\rho\dot{h})} d(r^2\rho w') = -\int_0^h \frac{\partial\rho}{\partial t}\,dz -$$

$$\frac{1}{r\sin\theta}\frac{\partial}{\partial\theta}\left[\int_0^h \rho u\sin\theta\,dz\right] -$$

$$\frac{1}{r\sin\theta}\frac{\partial}{\partial\varphi}\left[\int_0^h \rho v\,dz\right].$$

Substituting Equation A-10 and A-11 into this equation, recalling Equation A-9 and performing the indicated integrations results in

$$\frac{1}{12r^2}\left\{\frac{1}{\sin\theta}\frac{\partial}{\partial\theta}\left[\frac{h^3\rho\sin\theta}{\mu}\frac{\partial p}{\partial\theta}\right] +\right.$$

$$\frac{1}{\sin^2\theta}\frac{\partial}{\partial\varphi}\left[\frac{h^3\rho}{\mu}\frac{\partial p}{\partial\varphi}\right]\Bigg\} = \frac{\partial}{\partial t}(\rho h) +$$

$$\frac{1}{2r\sin\theta}\left\{\frac{\partial}{\partial\theta}\left[u_h h\rho\sin\theta\right] + \frac{\partial}{\partial\varphi}\left[v_h h\rho\right]\right\},$$

which is the Reynolds equation in spherical coordinates.

This equation may be nondimensionalized by multiplying through by $\mu_2/h_r^3\rho_2 p_2$ and letting

$$H = \frac{h}{h_r},$$

$$P = \frac{p}{p_2},$$

$$T_\omega = \omega t,$$

$$U = \frac{u_h}{v_r},$$

$$V = \frac{v_h}{v_r},$$

$$\Gamma = \frac{\rho}{\rho_2}, \text{ and}$$

$$\Omega = \frac{\mu}{\mu_2} ,$$

which yields

$$\csc\theta \frac{\partial}{\partial\theta}\left[\frac{H^3\Gamma}{\Omega}\sin\theta\frac{\partial P}{\partial\theta}\right] + \csc^2\theta\frac{\partial}{\partial\varphi}\left[\frac{H^3\Gamma}{\Omega}\frac{\partial P}{\partial\varphi}\right]$$

$$= \frac{\Lambda}{\sin\theta}\left\{\frac{\partial}{\partial\theta}(U\Gamma H\sin\theta) + \frac{\partial}{\partial\varphi}(V\Gamma H)\right\} + \sigma\frac{\partial}{\partial T_\omega}(\Gamma H) ,$$

(A-12)

where the compressibility number Λ and the squeeze number σ are defined as

$$\Lambda = \frac{6\mu_2 r v_r}{h_r^2 p_2} ,$$

$$\sigma = \frac{12\mu_2 r^2\omega}{h_r^2 p_2} .$$

The unknowns in Equation A-12 are p, ρ, μ, and h. The radial clearance, h, will either be assumed constant or a variation with θ and φ specified. The Reynolds equation, Equation A-12 and the energy equation, Equation A-4, are coupled due to the unknown dependency of ρ and μ on p and T. In order to obtain the pressure profile for compressible

flow it is necessary to solve these equations simultaneously. Such solutions are difficult to obtain as they require numerical methods.

It is well known that the viscosity μ is comparatively insensitive to small changes in temperature and only slightly affected by pressure; therefore, for most gas lubricating films μ may be considered constant. If it is assumed that the gas expands polytropically as did Comolet (15), the energy equation may be replaced by the approximation,

$$\frac{p^{\frac{1}{n}}}{\rho} = K.$$

If

$$K = \frac{p_2^{\frac{1}{n}}}{\rho_2},$$

this relation becomes

$$\Gamma = p^{\frac{1}{n}}.$$

Substituting this nondimensional relation into Equation A-12,

$$\frac{\csc\theta}{\Omega}\frac{\partial}{\partial\theta}\left[H^3 \sin\theta\, p^{\frac{1}{n}}\frac{\partial P}{\partial\theta}\right] +$$

$$\frac{\csc^2\theta}{\Omega}\frac{\partial}{\partial\varphi}\left[H^3P^{\frac{1}{n}}\frac{\partial P}{\partial\varphi}\right]=\frac{\Lambda}{\sin\theta}\left\{\frac{\partial}{\partial\theta}\left(UP^{\frac{1}{n}}H\sin\theta\right)+\frac{\partial}{\partial\varphi}\left(VP^{\frac{1}{n}}H\right)\right\}+\sigma\frac{\partial}{\partial T_\omega}\left(P^{\frac{1}{n}}H\right)\ . \qquad \text{(A-13)}$$

This equation will yield only approximate pressure profiles due to the polytropic flow approximation.

Grinnell (22) solved the momentum and energy equations simultaneously to obtain a solution for the longitudinal gas flow between parallel walls. Huges, in a discussion of this paper, observed that the temperature remained constant in the adiabatic parallel surface film. The isothermal condition has been verified through experimental evidence by Grinnel (22), Comolet (15), and many other authors for both longitudinal and radial flow.

For isothermal conditions the Reynolds Equation becomes:

$$\frac{\csc\theta}{\Omega}\frac{\partial}{\partial\theta}\left[H^3\sin\theta\,P\frac{\partial P}{\partial\theta}\right]+\frac{\csc^2\theta}{\Omega}\frac{\partial}{\partial\varphi}\left[H^3P\frac{\partial P}{\partial\varphi}\right]=\frac{\Lambda}{\sin\theta}\left\{\frac{\partial}{\partial\theta}(UPH\sin\theta)+\frac{\partial}{\partial\varphi}(VPH)\right\}+\sigma\frac{\partial}{\partial T_\omega}(PH)\ . \qquad \text{(A-14)}$$

This nonlinear partial differential equation is the basis of the viscous lubrication theory in spherical coordinates. It may be simplified for given bearing configurations by using arguments of symmetry and by placing restrictions on the relative surface motion of the bearing. Such restrictions have been used in Chapter III.

APPENDIX B

MODIFIED JOURNAL BEARING

The restrictor of the journal bearing shown in Figure 1, page 2, was modified according to the results obtained in the previous investigation to inherent compensating without a pool. This was accomplished, as shown in Figure 25, by counterboring the flat areas of each bearing pad surface and installing threaded plugs. These plugs were successfully lapped into the spherical contour without disturbing the remaining bearing surface. Inherent restrictors 0.025 inches in diameter were used in this bearing.

The modified journal bearing was loaded in the axial direction and the results are presented in Figure 26, page 109, The two theoretical load capacity curves presented in this figure were obtained through the use of the simplified journal bearing model and pad load characteristics for either variable radial clearance (Equation 31) or constant radial clearance (Equation 32). The experimentally determined journal bearing load characteristics agree well with theoretical predictions for variable radial clearance. This is to be expected since the journal bearing is deflecting in excess of 80 per cent of the large zero load constant radial celarance (c = 0.0015 inches). The load reducing effects of

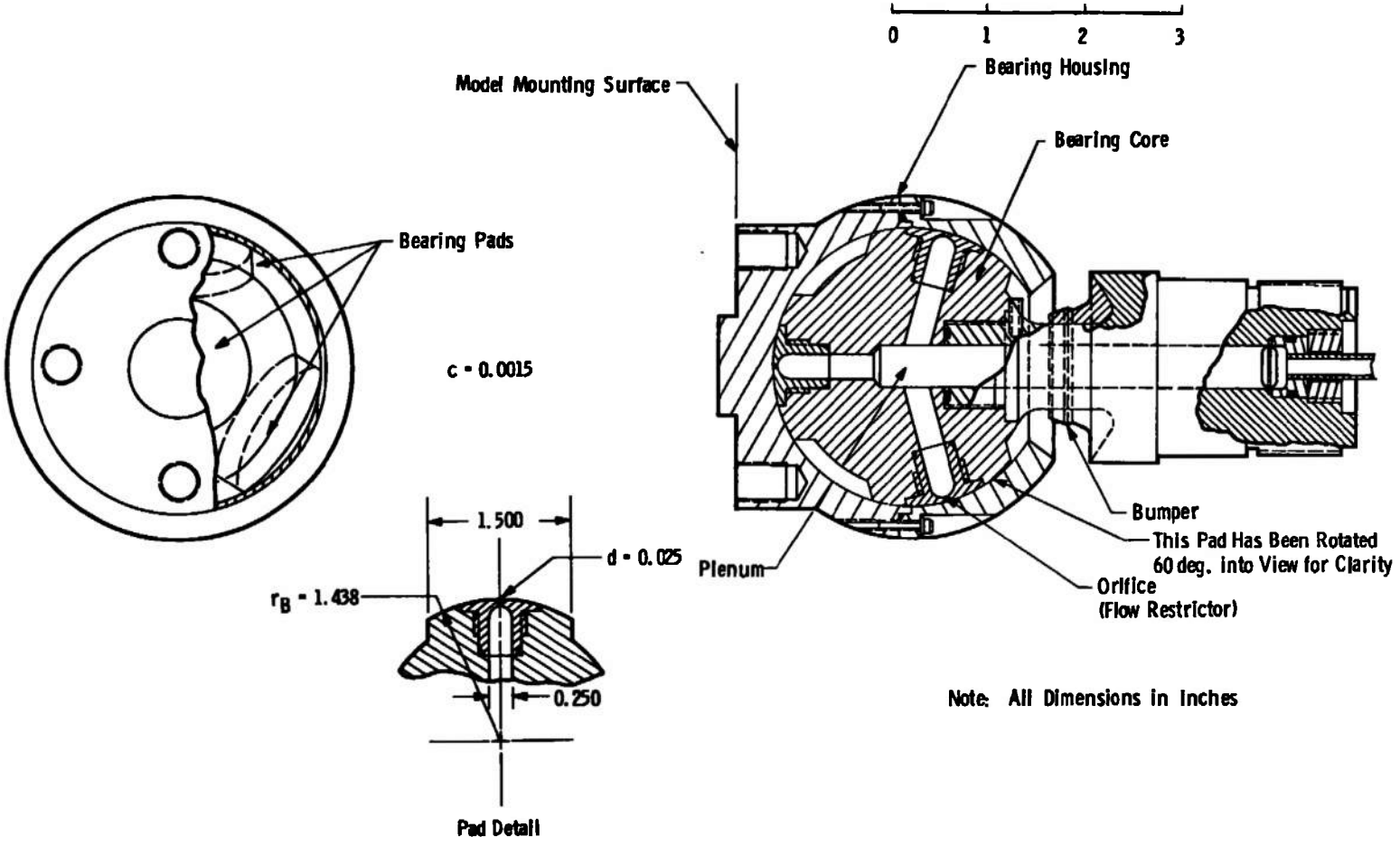

Figure 25. Modified journal bearing.

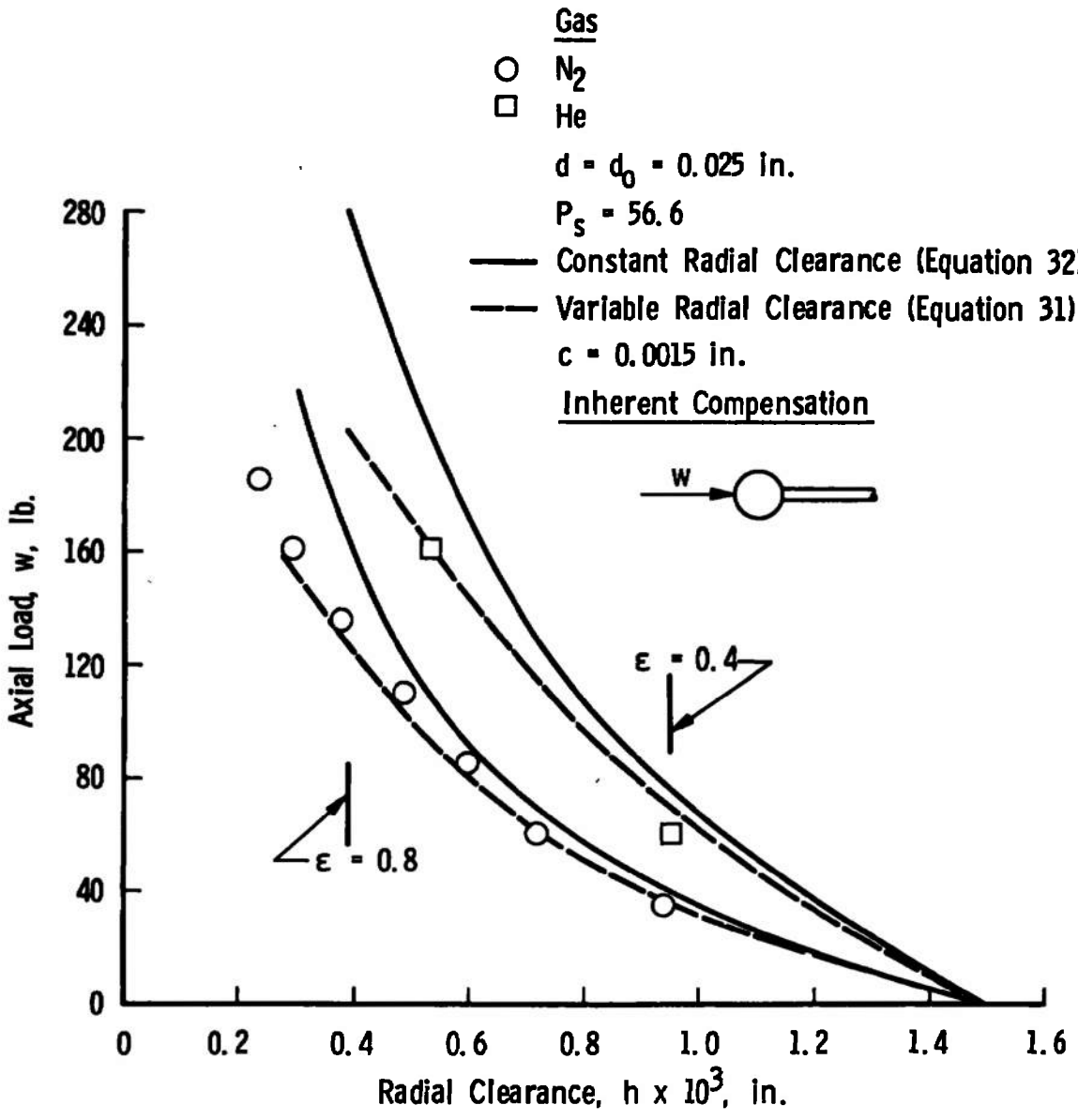

Figure 26. Modified journal bearing performance under an axial load.

large eccentricity ratios are demonstrated in this figure by the difference in the theoretical values for constant and variable radial clearance. Using h = 0.0003 inches as the minimum radial clearance, the maximum load carrying capacity of the bearing in the axial direction is 160 pounds when nitrogen is used. Helium is shown to yield a significant increase in load carrying capacity over nitrogen; however, it is not practical to use it due to its high cost caused by nonrecovery.

The results presented in Figure 27 were obtained by loading the journal bearing in a direction normal to its axis of symmetry. When loaded in this manner there is no symmetry in the lubricating film over the pads. For this case the film can be thought of as having eccentricities in two orthogonal directions. Comparing the results for the axial loading given in Figure 26, page 109, and those for the normal loading given in Figure 27 it is shown that in general this complicated film geometry causes a reduction in load capacity. As shown in Figure 27 the minimum load capacity occurs when the load vector passes between two pads. Using h = 0.0003 inches as the minimum allowable radial clearance, the maximum load carrying capacity of the bearing in the normal direction is 100 pounds when nitrogen is used. Here again helium yields a substantial increase in load carrying capacity.

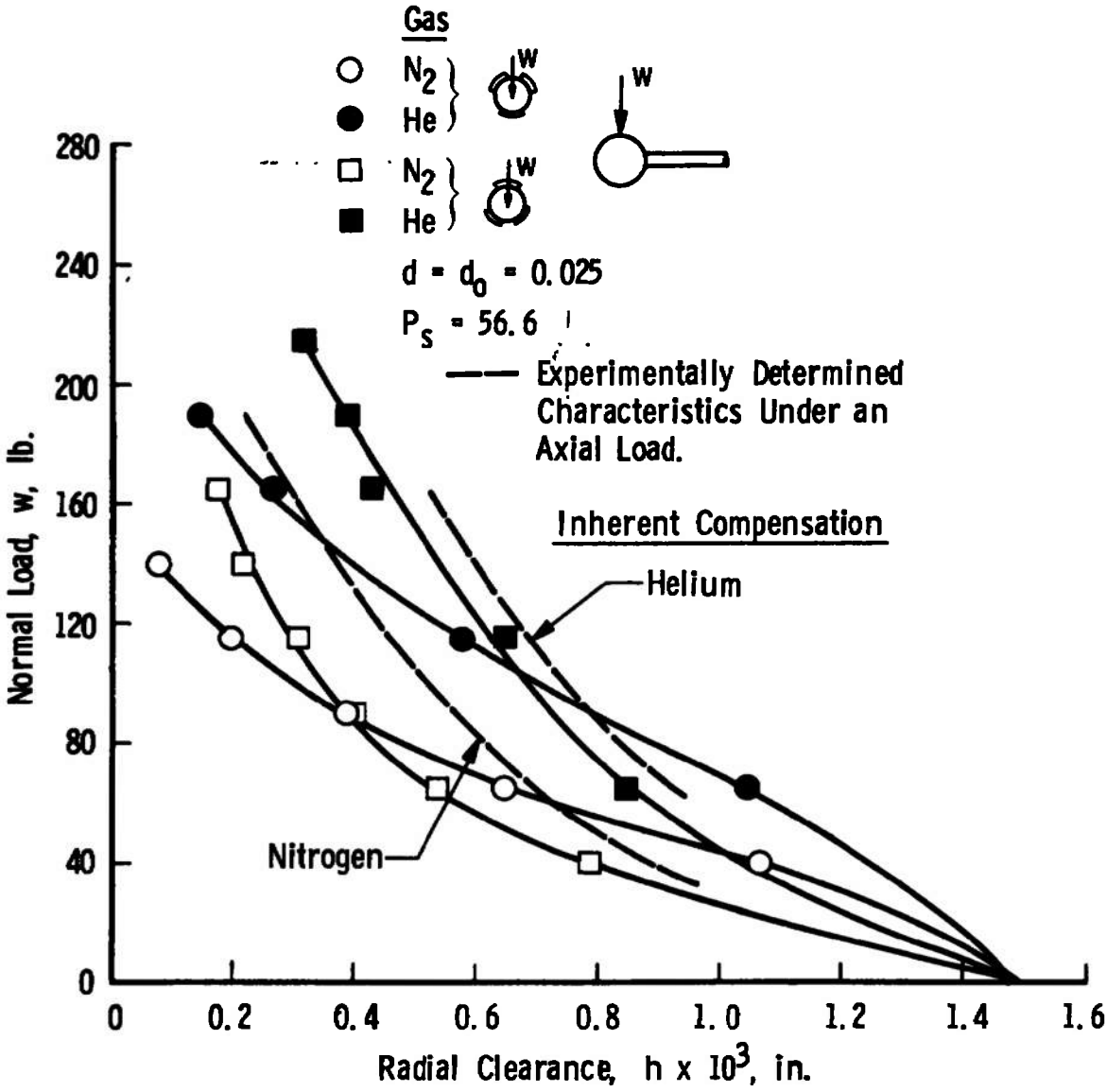

Figure 27. Modified journal bearing performance under a normal load.

Security Classification

DOCUMENT CONTROL DATA - R & D

(Security classification of title, body of abstract and indexing annotation must be entered when the overall report is classified)

1. ORIGINATING ACTIVITY (Corporate author)	2a. REPORT SECURITY CLASSIFICATION
Arnold Engineering Development Center ARO, Inc., Operating Contractor Arnold Air Force Station, Tennessee	UNCLASSIFIED
	2b. GROUP N/A

3. REPORT TITLE

A THEORETICAL AND EXPERIMENTAL INVESTIGATION OF A SPHERICAL GAS JOURNAL BEARING

4. DESCRIPTIVE NOTES (Type of report and inclusive dates)
June 1965 to June 1967 Final Report

5. AUTHOR(S) (First name, middle initial, last name)

A. E. Hodapp, Jr., ARO, Inc.

6. REPORT DATE	7a. TOTAL NO. OF PAGES	7b. NO. OF REFS
October 1967	121	22

8a. CONTRACT OR GRANT NO.	9a. ORIGINATOR'S REPORT NUMBER(S)
AF 40(600)-1200 b. PROJECT NO. 06RB	AEDC-TR-67-222
c. Program Element 6540223F	9b. OTHER REPORT NO(S) (Any other numbers that may be assigned this report) N/A
d.	

10. DISTRIBUTION STATEMENT
This document has been approved for public release and sale; its distribution is unlimited.

11. SUPPLEMENTARY NOTES	12. SPONSORING MILITARY ACTIVITY
Available in DDC	Arnold Engineering Development Center Air Force Systems Command Arnold Air Force Station, Tennessee

13. ABSTRACT An externally pressurized spherical gas journal bearing, which has multiple spherically surfaced pads, was designed and fabricated for use as a three degree-of-freedom pivot which will support large loads (100 lbs). This inherently compensated pool type bearing design proved to be pneumatically unstable. The problem then was to determine a restrictor configuration for this bearing which would insure pneumatic stability and a large load carrying capacity. Restrictor configurations investigated were inherent compensating both with and without a pool and orifice compensating without a pool. The Reynolds equation and the equations for the distributed film velocities are developed in the report for spherical coordinates. Using these equations, theoretical estimates of bearing pad static characteristics (load carrying capacity, stiffness, etc.) were obtained for the above listed restrictor configurations. The problem of pneumatic instability was investigated using information available in the literature. The operating conditions of the bearing are such that the theoretical predictions are subject to question. A model bearing, which duplicates the lubricating film of a journal bearing pad, was, therefore, constructed in order to obtain experimental data to verify the theoretical predictions. For this particular bearing configuration operating at large supply pressures (800 psig), it was found that an inherent compensating restrictor without a pool will ensure pneumatic stability and maximum load carrying capacity. This result is in agreement with theoretical predictions of dynamic behavior and is in disagreement with theoretical predictions of load carrying capacity.

DD FORM 1 NOV 68 1473

Security Classification

Security Classification

14. KEY WORDS	LINK A		LINK B		LINK C	
	ROLE	WT	ROLE	WT	ROLE	WT
1 gas journal bearing pneumatic stability restrictor configurations 2. Gas bearing 11-2						

Security Classification